

1 Decadal-Scale Relationship Between Measurements of Aerosols, Land-Use Change, and Fire over
2 Southeast Asia

3 Jason Blake Cohen^{1*}, Eve Lecoœur², and Daniel Hui Loong Ng²

4 [1] School of Atmospheric Sciences, Sun Yat-Sen University, Guangzhou, China

5 [2] Tropical Marine Sciences Institute, National University of Singapore, Singapore

6 * Corresponding Author: Jason Blake Cohen (email: jasonbc@alum.mit.edu)

7 **Abstract.**

8 A simultaneous analysis of 13 years of remotely sensed data of land cover, fires,
9 precipitation, and aerosols from the MODIS, TRMM, and MISR satellites and the AERONET
10 network over Southeast Asia is performed, leading to a set of robust relationships between land-use
11 change and fire being found on inter-annual and intra-annual scales over Southeast Asia, reflecting
12 the heavy amounts of anthropogenic influence over land use change and fires in this region of the
13 world. First, we find that fires occur annually, but with a considerable amount of variance in their
14 onset, duration, and intensity from year to year, and from two separate regions within Southeast
15 Asia from each other. Second, we show that a simple regression-model of the land-cover, fire, and
16 precipitation data can be used to recreate a robust representation of the timing and magnitude of
17 measured AOD from multiple measurements sources of this region using either 8-day (better for
18 onset and duration) or monthly based (better for magnitude) measurements, but not daily
19 measurements. We find that the reconstructed AOD matches the timing and intensity from
20 AERONET measurements to within 70% to 90% and the timing and intensity of MISR
21 measurements from to within 50% to 95%. This is a unique finding in this part of the world, since
22 cloud-covered regions are large, yet the model is still robustly capable, including over regions
23 where no fires are observed and hence no emissions would be expected to contribute to AOD. Third,
24 we determine that while Southeast Asia is a source region of such intense smoke emissions, that
25 portions of it are also impacted by smoke transported from other regions. There are regions in
26 Northern Southeast Asia which have two annual AOD peaks, one during the local fire season, and
27 the second smaller peak corresponding to a combination of some local smoke sources as well as
28 transport of aerosols from fires in Southern Southeast Asia, and possibly even from anthropogenic
29 sources in South Asia. Overall, this study highlights the importance of taking into account a
30 simultaneous use of land-use, fire, and precipitation for understanding the impacts of fires on the
31 atmospheric loading and distribution of aerosols in Southeast Asia over both space and time.

32 Furthermore, it highlights that there are significant advantages using 8-day and monthly average
33 values (instead of daily data), in order to better quantify the magnitude and timing of Southeast Asia
34 fires.

35 **1 Introduction**

36 Southeast Asia has been experiencing major haze events over the past three to five decades,
37 due to a combination of increased urbanization (Cohen and Wang, 2014; Cohen and Prinn, 2011)
38 and large-scale conversion of forests by fire (Cohen, 2014; van der Werf et al., 2008; Taylor, 2010;
39 Dennis, 2005). The underlying connections and mechanisms relating the sources and strength of
40 fire-based emissions and observed intra-annual, inter-annual, and inter-decadal variations of fire
41 events, with meteorology, land-use change, and anthropogenic driving factors are not well
42 understood (van der Werf et al., 2006; Giglio et al., 2006; Hansen et al., 2008; Field et al., 2009).
43 Moreover, recent studies have shown that the impacts these events have on the atmospheric loading
44 of aerosols and the larger climate are becoming greater in both absolute terms and frequency
45 (Langmann et al., 2009; Nakajima et al., 1999; Podgorny et al., 2003; Rosenfeld, 1999). Some of
46 the heaviest events, which previously in the literature were only associated only with strong El-
47 Nino induced drying events, are now being found to occur in connection with other, less extreme
48 impacts on precipitation and even surface moisture, occurring at various scales including but not
49 limited to the Indian Ocean Dipole, the Madden-Julian Oscillation, the shifting of the Inter-Tropical
50 Convergence Zone, mountain induced waves, the land-sea breeze and localized convection (Fuller
51 and Murphy, 2006; Wooster et al., 2012; Natalia Hasler and Avissar, 2009; Reid et al., 2013). The
52 fact that so many factors are capable of influencing these large-scale events is likely to make
53 prediction much more challenging, as is seen by the fact that since 2000, there were extreme events,
54 of varying intensity, length, and duration, occurring in 2002, 2004, 2006, 2009, 2013, and 2014 in
55 Southern Southeast Asia, the region covering Indonesia, Malaysia, Singapore, and Brunei, and
56 every year except 2003 in Northern Southeast Asia, the region covering Thailand, Myanmar,
29 Cambodia, Vietnam, and Laos (Neale and Slingo, 2003; Chang et al., 2005; Aldrian et al., 2007;
57 Cohen, 2014; Wooster et al., 2012). To date, other than (Cohen, 2014), there have been no other
58 studies that have looked at Southeast Asian fires both robustly and holistically, to the extent of being

59 able to reproduce both the extreme and low levels of aerosols at both the monthly and the decadal
60 scale. Furthermore, other than (Cohen, 2014; Cohen and Wang, 2014) there are no other works that
61 have been able to satisfactorily estimate the emissions of aerosols over this region of the world,
62 from the fundamentals and over the entire time period, without scaling or other statistical
63 enhancement techniques, to match with atmospheric column measurements, such as aerosol optical
64 depth (AOD) and absorbing aerosol optical depth (AAOD).

65 Knowledge of the spatial, temporal, and magnitude of the emissions and atmospheric
66 loadings is essential for our improved understanding of the environmental impacts of the fires.
67 Emissions of aerosols and gases from these fires, include significant sources of black carbon (BC),
68 organic carbon (OC), and ozone, and therefore contribute greatly towards impacting human health
69 (Afroz et al., 2003), atmospheric radiative forcing (Wang, 2007; Jacobson, 2001; Ming et al., 2010;
70 Ramanathan and Carmichael, 2008; Cohen et al., 2011), and cloud and precipitation properties
71 (Huang et al., 2006; Tao et al., 2012; Wang, 2013). Furthermore, given the general circulation of the
72 Earth, and the lack of precipitation during the dry season in the tropics, coupled with intense
73 localized convection, a large portion of the emitted pollutants will spread widely in space and time,
74 entering into the global-scale circulation patterns (Wang, 2007). Therefore, emissions from these
75 regions during these times of the year may have a significant impact on people and the environment
76 thousands of kilometers away from their source.

77 AOD can be used to quantify the emissions from the fires, since it is the non-dimensional
78 vertical integral of the atmospheric extinction (the sum of scattering and absorbance) of solar
79 radiation due to aerosols. AOD is useful since it can be measured by a combination of land-based
80 and space-borne instruments (Holben et al., 1998; Petrenko et al., 2012; Dubovik et al., 2000). The
81 extinction is in turn a function of the vertical aerosol mass and size distributions as well as
82 chemical, physical, and optical properties. These values in turn are a function of the emissions and
83 gasses from fires and other various anthropogenic sources, in-situ processing, washout from

84 precipitation, and atmospheric transport. Hence, the emissions of primary BC and OC from these
85 fires, coupled with other secondary species, has a functional relationship with the change in the
86 AOD, which otherwise would not have occurred over these fire regions and downwind, at these
87 specific times, if the fires were not present.

88 This paper uses these relationships and goes one step further, to make the link between
89 measurements of land-use change and fires directly with the atmospheric column measurements,
90 with fires the intermediary step between the two. This is because rapid conversion of forests,
91 agricultural lands, and associated waste products by burning is one of the primary sources of
92 aerosols throughout Southeast Asia (Langmann et al., 2009; Miettinen et al., 2013). However, little
93 is known about the exact spatial and temporal distribution of these fires (Fu et al., 2012; Chen et al.,
94 2016; Zhou et al., 2016). Furthermore, the inter-annual and intra-annual variability of biomass
95 burning and its associated underlying mechanisms are also not well understood or constrained by
96 measurements, leading to the current poor understanding of fires impact on the local and global
97 aerosol climatology (van der Werf et al., 2006). Furthermore, Southeastern Asia is often covered
98 with clouds, which further complicates detecting both fire and the pollution that comes from it
99 (Miettinen et al., 2013; Giglio et al., 2006; Remer et al., 2013). A few studies have looked at this
100 and give estimates that the emissions are underestimated, up to a factor of 4 times (Giglio et al.,
101 2003, 2006; Petrenko et al., 2012; Cohen, 2014; Cohen and Wang, 2014).

102 Given that large-scale fires lead to abrupt and definitive changes in the vegetative properties,
103 we employ a set of measures of land surface properties which have a long time-record, such as LAI
104 (Leaf Area Index), NDVI (Normalized Difference Vegetation Index), and the number of 1km by
105 1km pixels with a measured fire (Fire Count). While we know that some changes may be masked,
106 obscured, or otherwise missing, any observed abrupt changes in these variables or the land's
107 properties itself must be linked at a minimum with any observed changes in the AOD itself.
108 Moreover, since the onset and the offset on the Asian Monsoon controls the start and end of the fire

109 seasons by rapidly changing from relatively dry to intensely wet and visa versa (Hansen et al.,
110 2008), large scale changes in the monthly-scale precipitation is a proxy for the ability of the fires to
111 occur, as well as washout of aerosols. Therefore, precipitation is also intimately linked with
112 measured AOD over Southeastern Asia. This is even more important given that there are only very
113 few studies that have been able to quantify emissions over this region successfully, over the decadal
114 scale, without resorting to statistical scaling, in relation to measured AOD and AAOD. Furthermore,
115 the few emissions datasets that have been made are not capable of working at a higher frequency
116 than monthly. Additionally, they have not been directly linked to the changes in the land surface
117 properties that should be driving them (Cohen and Wang, 2014; Cohen, 2014).

118

119 **2 Data and Methods**

120 Several remotely sensed and surface measurements of the surface land properties (LAI and
121 NDVI), the number of active fires (Fire Count), aerosol (AOD), and precipitation (rainfall) are used
122 in this study. These are used in conjunction with advanced analytical procedures to determine the
123 regions which contribute the most to the variance of the impact of fires on the atmosphere loading
124 of aerosols as observed by the AOD. This analysis, in addition to its own results, leads to the
125 production of a simple statistical multi-year constrained model, which is shown to be capable of
126 reproducing the AOD as a function of the land use, fire, and precipitation measurements, even in
127 additional years, and even as tested against measurements of AOD from different sources. All of the
128 details of the measurements used, the procedures and methods employed, and the statistical and
129 analytical techniques employed are detailed below.

130

131 **2.1 Geography**

132 The domain of interest for this study is Southeast Asia, which we define here as the region
133 spreading from 90°E to 130°E in longitude, and from 14°S to 23°N in latitude (see Figure 1). The

134 subregion defined as Northern Southeast Asia is defined by a mostly large continental land masses
135 and a single Wet Season each year, and consists of Thailand, Myanmar, Cambodia, Laos, Vietnam,
136 and parts of Southern Greater China. The subregion defined as Southern Southeast Asia is defined
137 by a mixture of land and water and has two Wet Seasons each year, and consists of Malaysia,
138 Indonesia, Brunei, and Singapore. Maps of the fires in January 2013 and September 2013
139 respectively are given in Appendices C1 and C2.

140

141 **2.2 Measured Data**

142 For the basic remotely sensed measurements used in the analysis, model construction, and
143 results, we use remotely sensed variables from the MODIS instrument on both the TERRA and
144 AQUA satellites. Measurements of AOD (Levy et al., 2013) are from Collection 6, Level 2 product,
145 swath-by-swath at 0.55 micron, and consist of both over land and over ocean, cloud-cleared pixels,
146 measured daily with a spatial resolution of 10km by 10km at nadir. Each swath of only quality
147 controlled pixels of AOD data, from January 1, 2001 through December 31, 2013, has been
148 interpolated onto a consistent and standardized 0.1° by 0.1° square grid.

149 It has been shown that there is a slightly biased uncertainty in the measurement of AOD of
150 $-0.02-0.10 \cdot \text{AOD} + 0.04+0.1 \cdot \text{AOD}$ over the ocean and $\pm 0.05+0.15 \cdot \text{AOD}$ over the land (Levy et
151 al., 2013; Sayer et al., 2012). However, over this region, the magnitude of the “noisy floor” is small
152 compared to the linear term, given that the AOD in polluted regions goes as high as 1.5 to 2.0. And
153 while this linear term seem to not be too small, it is actually quite small compared to the difference
154 between the peaks and the troughs as obtained by the variance maximizing technique. Additionally,
155 as shown by (Cohen and Wang, 2014) and others, this error is sufficiently small as to not impact the
156 end results, especially when compared with the uncertainties in the current best-generation of
157 models and the dynamics of the atmosphere itself. In these cases, the models tend to be lucky to
158 obtain measurements within a 20% to 30% range of the measurements, and often perform more

159 poorly than this (e.g. Cohen and Prinn, 2011; Cohen and Wang 2014). AOD is a measure of the
160 vertical sum of the extinction of sunlight (scattering plus absorption) through the atmosphere due
161 to aerosol particles, and therefore is a function of the atmospheric loading of aerosols, washout
162 from precipitation, and the vertical, size, and optical properties of the aerosols. Hence, there is a
163 physical relationship between measured changes in AOD and the emissions and subsequent in-situ
164 atmospheric processing of aerosols. It has been shown that strong spatial and temporal variability in
165 AOD measurements over this part of the world are due to biomass burning from this region of the
166 world, while large measurements of AOD which mostly only co-vary only with precipitation
167 (washout) are more consistent with urban emissions (Cohen, 2014; Cohen and Wang, 2014).

168 To estimate the land-surface and fire responses we also use the measured values of LAI,
169 NDVI, and Fire Count from MODIS (Nightingale et al., 2008; Yang et al., 2006; Huete et al., 1999;
170 Giglio et al., 2003). Measurements of LAI and Fire Count (Collection 5.1, Level 2 product) are
171 made on an 8-day average basis at 1km by 1km horizontal resolution. While for NDVI the
172 measurements are on a 16-day average basis at 1km by 1km horizontal resolution. Each product is
173 then aggregated onto the same consistent and standardized 0.1° by 0.1° square grid used for the
174 AOD. All measurements only use data which has been quality assured to be cloud free. However, in
175 this region, there are some optically thin clouds that will not be picked up, and this may
176 significantly bias the measurements of Fire Count, which are inherently based on IR measurements,
177 but should not be as impacting on LAI and NDVI, which both depend mostly on measurements in
178 the visible bands.

179 LAI is chosen since it represents the amount of leaf material in an ecosystem and hence is
180 useful both for identifying if there was a sudden change in the amount of vegetation available and
181 its condition (Asner et al., 2003), such as expected after leaves are consumed in a fire. It is
182 geometrically defined as the total one-sided area of photosynthetic tissue per unit ground surface
183 area. LAI values range from 0 for bare ground, to the range of 1 to 4 for grassland and crops, to the

184 range of 5 to 9 for plantations, and as high as 10 for dense conifer forests. One of the large
185 drawbacks of using LAI in this region of the world is that it is hard to analyze the variance in the
186 LAI over areas that are used for non-forest agriculture. This is because the LAI is considerably
187 lower than the tropical primary and secondary forests. Hence, after a burning event, the absolute
188 magnitude of the LAI and hence the amount of variance is lower. Yet, this is the more robust land
189 surface variable, given that it uses many of the wavebands from MODIS. For this reason, the
190 variance in the LAI is most helpful in determining deforestation from fire, particularly in regions
191 which are not found to have hotspots.

192 Fire Count determines how many of the pixels within the area have an active fire. It is based
193 on a two factors, first if there is a sufficient amount of infrared emissions to determine that there is
194 an absolute detection of a fire of sufficient strength. The second factor is whether the detected
195 surface temperature is sufficiently variable as compared to the surrounding pixels. Given the
196 complexity involved with using infrared and visible streams for the fire count, as well as the
197 possibility of thin clouds obstructing this measurement, we only use quality assured Fire Count
198 values, those with a value corresponding to 7 or more. In this study, it is found that the number of
199 Fire Count can vary from 0 to more than 5000 (with a corresponding value of 8) or more than 600
200 (with a corresponding value of 9) on a monthly basis.

201 NDVI is also chosen since it represents a measure of the health of the vegetation. NDVI is
202 mathematically calculated from the visible (VIS) and near-infrared light reflected(NIR) by the
203 vegetation as follows: $NDVI = \frac{NIR - VIS}{NIR + VIS}$. Healthy vegetation absorbs most of the visible light that
204 hits it, and reflects a large portion of the near-infrared light. On the other hand, unhealthy or
205 sparsely healthy vegetation, such as after being burned, reflects more visible light and less near-
206 infrared light. Given this formula, a value close to zero (-0.1 to 0.1) implies that there the land is
207 barren with respect to living and green vegetation, whereas values close to +1.0 correspond to the
208

209 highest density of healthy green leaves. NDVI is an ideal way to search for the ratio of the
210 magnitude of the variance to the absolute mean. This is because the variance in the change in the
211 health is actually proportionate to the initial value. In this case, while the overall variance is not too
212 much throughout the region, the ratio is considerably high in regions which undergo rapid change
213 such as from burning. However, such changes are not very useful for looking at small changes over
214 large periods of time, and more are useful at looking at changes occurring over short periods of
215 time. This is one way to overcome the issue of regeneration, either due to natural regrowth or due to
216 anthropogenic planting.

217 Furthermore, since the onset of the monsoon brings sufficiently large amounts of
218 precipitation that it usually leads to the end of the fire season (Cohen, 2014; Natalia Hasler and
219 Avissar, 2009), knowledge of the rainfall rate is important. For this, we use TRMM measurements
220 of precipitation, as generated by the 3B42 algorithm. This produces daily average precipitation
221 measurements at 0.25° by 0.25° spatial resolution over the areas of interest for this work.

222 To validate the results, we also use two additional measurement platforms for AOD from
223 AERONET and MISR. From AERONET (Holben et al., 1998) we either use available AOD at 0.55
224 microns or interpolate the surrounding wavelength-specific measurements to 0.55 microns, at 9
225 different stations located in the region of interest. We use all individual Level 2.0 data points, cloud
226 screened and validated, and then averaged to form a daily value, where a sufficient amount of data
227 is available. At the four stations where there is insufficient data, we use individual Level 1.5 data
228 points. However, before forming the daily average value in the case of Level 1.5 data, we only
229 retain the AOD measurements when the corresponding Angstrom Exponent is larger than 0.2,
230 giving us reassurance that the product is relatively cloud-free. This has been tested by varying the
231 sensitivity from 0.1 to 0.4 (the minimum physically acceptable value must be positive) and there is
232 little change in the end result. Although AERONET is the most precise measurement platform for
233 AOD, it is limited in spatial coverage. Therefore we also use measurements from MISR (Diner et

234 al., 1998; Kahn et al., 2010) of AOD at 0.55 microns, with a monthly temporal resolution and a 0.5°
235 by 0.5° spatial resolution. The reason for choosing MISR is that it has a smaller error with respect to
236 AERONET over this region of the world than any other satellite platform, (Petrenko and Ichoku,
237 2013) which allows us to provide spatially distributed validation. Although MISR has a more
238 narrow swath-width than MODIS, in this region of the world, there are actually more data points
239 that are retrieved at the AERONET stations and that the error is lower in comparison to the
240 AERONET Measurements. This is partially due to the fact that it is able to cloud process and clear
241 more efficiently than MODIS due to the spherical fraction. Additionally, the fact that MISR is able
242 to measure AOD levels greater than 2.0 allows it to actually obtain more pixels on a monthly basis
243 over this region than MODIS. However, the major downside is that only at a monthly average or
244 lower frequency is available, with the monthly dataset having from 4 to 8 data points per
245 measurement. It is therefore effective over this region at obtaining a spatial distribution upon which
246 to extend the more precise AERONET results. However, this helps quite a bit with the cloud
247 clearing statistics. Combining these together allows the use of the higher quality AERONET data as
248 an anchor, where it is available, to evaluate any errors in the magnitude between the model and the
249 measurements, even away from the source, so long as it is still in the same geographical region (as
250 described below). It also provides a means for investigating how error propagation between various
251 different measurement sources can be quantified.

252 All of the data used has been taken from from January 2001 through December 2013. In the
253 case of remotely sensed data, it was first interpolated (in the case of AOD) or aggregated (in the
254 case of Fire Count, NDVI, and EVI) onto a 0.1° by 0.1° square grid, using only quality assured
255 data. These gridded, data sets, were then aggregated or interpolated respectively to the temporal
256 resolution used, either 1-day, 8-day, or monthly average temporal resolution, to make them
257 consistent. AERONET measurements have also been taken using whatever data was available over
258 the same respective 1-day, 8-day, and monthly periods, and have been considered to be

259 representative of the entire corresponding 0.1° by 0.1° box in which they are located. One of the
260 significant advances of using this approach is the ability to analyze how the results are improved by
261 using data with different temporal variability.

262

263 **2.3 Variance Maximizing Technique**

264 Aerosol emissions and resulting changes in AOD in the Southeastern Asia region mainly
265 comes from two types of sources: urban/anthropogenic and fires. Emissions of aerosols from urban/
266 anthropogenic include those from cities, transportation, and industrial processes, which generally
267 include temporally and geographically regular combustion of coal, oil, and natural gas throughout
268 the year. On the other hand, emissions of aerosols from fires, which include clearing of forests,
269 agriculture, peat, and rubbish, are more highly irregular over space and time, preferentially
270 occurring under certain economic conditions as well as during periods of dryness, due to either
271 changes in irrigation or under the influence of various meteorological/climatological conditions
272 (Cohen, 2014). As the ultimate goal of this study is to develop an understanding and constraint on
273 the absolute source of aerosol emissions, and since fire is the most uncertain contribution in this
274 region, therefore the analytical technique must target the large amount of variance in the measured
275 fields of the AOD. Those regions which both contribute the most to the variance of the AOD field as
276 well as correspond to a large annual amount of AOD on an absolute basis, are the regions which
277 which are most likely fires. A simple check of the geography has been performed to eliminate any
278 false positives that are known to be urban or industrial regions, of which there are at least 3 in the
279 regions under study: in Vietnam, Indonesia, and Malaysia. However, it is possible that rapidly
280 developing industrial uses of the land, such as new large mill-towns in Indonesia (as witnessed by
281 the author), were not fully identified. Further, observed land-use changes were considered to be
282 reasonable if they corresponded to reasonable changes in the values of NDVI and LAI.

283

284 To achieve these goals, we first employ the Empirical Orthogonal Functions/Principal
 285 Component Analysis technique (EOF/PCA) on the 8-day average AOD product. This is one of the
 286 beautiful things about using the EOF approach: patterns in the variance of the data search for the set
 287 of the relative maxima. Therefore, since the process searches for the highest and lowest values and
 288 gradients in space and time, any unbiased error in the measurements, will not significantly impact
 289 the result. Furthermore, the 8-day average product was chosen, so that it could take full advantage
 290 of the higher frequency of the MODIS data, when compared with the MISR data. Additionally, the
 291 lifetime of the aerosol plume is roughly on order of this period of time, given the low amount of
 292 precipitation and the high amount of aerosols lofted into the atmosphere due to the heat from the
 293 fires, making source/sink and overall statistical properties robust (Cohen, 2014; Lin et al., 2009; Lin
 294 et al., 2014).

295 The specific EOF/PCA analysis decomposes the 8-day AOD data F into subcomponents.
 296 Each subcomponent is orthogonal to the whole, and can be ordered based on the overall
 297 contribution to the fractional amount of the overall variability (Bjornsson and Venegas, 1997). This
 298 is done by decomposing the measurements into independent (orthogonal) spatial/geographic modes
 299 S_i and their associated temporal/time modes T_i , as explained in **EQUATIONS 1-5**, where a_{ij} are
 300 the individual measurements (i is the marker indicating the ordered number in latitude/longitude,
 301 and j is the individual marker indicating the marker in time), and c_i and y_i which are the
 302 corresponding decomposed values of the spatial and temporal maps accordingly.

$$F = \begin{pmatrix} a_{11} & \cdots & a_{1M} \\ \vdots & \ddots & \vdots \\ a_{N1} & \cdots & a_{NM} \end{pmatrix} \quad (1)$$

$$F^T F = C Y^T Y C^T \quad (2)$$

$$S_i = \begin{pmatrix} c_{1i} \\ \vdots \\ c_{Mi} \end{pmatrix} \quad (3)$$

$$T_i = \begin{pmatrix} y_{1i} \\ \vdots \\ y_{Ni} \end{pmatrix} \quad (4)$$

$$F = YC^T = T_1S_1^T + \dots + T_N S_N^T \quad (5)$$

303

304 **2.4 Regression-Fit Model Connecting Land Use Change to AOD**

305 Along with the analysis, we also employ a simple multi-variable linear regression model to
 306 predict AOD from measured land-use and meteorological variables. This approach is adapted
 307 because of the physical nature of the relationship between these variables. Fires lead to a direct drop
 308 in LAI in currently growing vegetation through the combustion process. In the case of agriculture
 309 which has already been harvested, the LAI would have previously dropped, while the dried products
 310 are left to burn. Similarly if there is a change in the vegetation/agricultural state after the fire, this
 311 should show up by a restored LAI, although at a different magnitude. NDVI would similarly be
 312 impacted, as the chlorophyll is combusted along with the plant material that is associated with it.
 313 Furthermore, the hypothesized loss of efficiency of the land surface associated with the fires would
 314 show up as a lower-frequency change in the NDVI. Due to these reasons, there may be a lag
 315 expected between the occurrence of the fire and the change in the land-use variable. However, given
 316 the rapid rate of regrowth over this region, and the high degree of cloud-cover, it is found that day-
 317 to-day passes or information are not very reliable. It is uncertain how much lag would be expected
 318 in weekly-averaged or two-weekly averaged products. Although our results have determined that in
 319

320 fact the relationship which is based on no lag produces the best fit. Hence, one of the objectives is
321 to quantify the impacts of different averaging kernels applied to the measurements.

322 There is also evidence that in regions where dryness is an issue, which it certainly is during
323 the extremes of the dry season throughout Southeast Asia, that NDVI recovers slower than LAI.
324 This would certainly be the case in regions in which peat is being drained or has recently been
325 drained, such as the Southern Southeast Asia Region, or in regions where there is little to no
326 irrigation, such as the Northern Southeast Asian Region (Hope et al, 2007; ; Morawitz et al., 2006;
327 Cuevas et al., 2008). The clear indication here is that the rate of greenness regrowth, as observed by
328 the change in the NDVI may not relate to the canopy and soil moisture regrowth, which is more
329 related to the LAI due to the additional bands in the NIR. However, in regions in the topics that are
330 either managed or are fed by the arrival of the monsoon, this is not expected to be a significant
331 issue, and hence a possible reason why little lag is actually observed.

332 During the dry season, based on how dry it is, will impact the amount, intensity, and
333 duration of the fires as a whole. In practice, years with wetter dry season or a drier dry season
334 should have a reduction in the intensity of the fires as well as their geographic spread, although it
335 will not necessarily lead to them being altogether suppressed. This relationship is slightly more
336 complex, since there are cases where anthropogenic water due to irrigation, burning occurring on
337 very wet peat, or fast-moving thunderstorms, can make the ground quite wet, but still continue to
338 burn, thereby leading to an increase in emitted aerosol, and hence AOD, due to a switch of the type
339 of fire from flaming to smoldering (Field et al., 2009; Saatchi et al., 2013). However, these cases are
340 over and beyond the approach taken here, and are still not yet fully understood. It is thought that
341 surface wetness is critical for this switch, although in theory this is partially a function of the LAI,
342 NDVI, and precipitation, and hence could be approximated to first order using the approach
343 employed here, with the physical variable itself at least being partially captured (Fisher et al., 2009;
344 Phillips et al., 2010; Wohl et al., 2012). Another advantage is that low-temperature fires, which may

345 otherwise go undetected, can still be represented, since they still impact changes in terms of AOD,
346 LAI, and NDVI.

347 To ensure that the impact of fires is physically as expected on AOD, in which an increase in
348 fire should lead to an increase in emissions and hence AOD, we employ two different regression
349 equations. Both equations use LAI, NDVI and Precipitation as predictive variables R2 (**Equation**
350 **7**), while only one R1 (**Equation 6**) also uses Fire Count. The regression coefficients α_i , β_i , γ_i , and
351 δ_i are computed by minimizing the root-mean-square errors of the equations **EQUATIONS 6,7**.
352 Using these constrained values, the AOD can be approximated during different seasons or over
353 different areas, such as those which are cloud-covered and hence do not show measurements. These
354 reconstructed values are generated and specifically compared against AOD values from other
355 measurement platforms, specifically MISR and AERONET.

$$356 \quad AOD_{MODIS,R1} = \alpha_1 * LAI + \beta_1 * NDVI + \gamma_1 * RAIN + \delta_1 * FireCount \quad (6)$$

$$357 \quad AOD_{MODIS,R2} = \alpha_2 * LAI + \beta_2 * NDVI + \gamma_2 * RAIN \quad (7)$$

358
359 Since the nature of the land-use change, the amount of precipitation, the state of native
360 vegetation, and the strengths and timing of the AOD signal are different over the two regions **S1** and
361 **S2**, we compute the fitting for AOD over each region separately. This helps us better quantify and
362 understand the functional relationships between these variables under the different land use types,
363 land-use management practices, and climatologies, when the fires actually do occur. This is
364 especially important in Southern Southeast Asia, where there is stronger year-to-year variability, the
365 issue of cloud-cover is much more pronounced close to the equator, there are only very few ground
366 station measurement sites, vastly different sets of anthropogenic land use policies in different
367 regions, and different magnitudes of fire emissions.

368 To test separately only the fire-occurring seasons, we define fire activity periods over each
369 region as the days during which which **T1** and **T2** respectively are above a certain threshold

370 τ_{North} and τ_{South} . Different thresholds for **T1** and **T2** are tested, based on the percentile **P** of the
371 time series beneath the point τ if the time series were to be regrouped and sorted. We hence use the
372 points $\mathbf{P}=\{0.90,0.835,0.75\}$. Since this method is testing for the extreme values in the AOD
373 variance, or when the fires are occurring, this method proves to be methodologically suitable, as it is
374 further providing a constraint on the more extreme conditions, and when the pattern is most
375 significant. The values chosen are not arbitrary, as they are based on the statistical robustness of the
376 magnitude of the fields $\mathbf{S}_i \cdot \mathbf{T}_i$. However, the point of the sensitivity analysis is to quantify at what
377 point the errors in the analytical technique are no longer able to statistically retrieve the maximum
378 contributions to the variance of signal, as compared to just picking up the variance induced by the
379 unbiased errors in the measurements themselves.

380

381 **3. Results**

382 **3.1 Decadal-Scale Analysis of Remotely Sensed Measurements of AOD and Land Surface**

383 **Properties**

384 The subsequent analysis performed using the variance maximizing analytical technique only
385 retains those modes $\mathbf{S}_i, \mathbf{T}_i$ that explain at least 5% of the total variability. This is to ensure that any
386 signal found is larger than the uncertainty in the measurements themselves, and hence should be
387 physically relevant. Specifically, since the MODIS AOD uncertainty is 5%, therefore we need at
388 least 5% of the variance for a mode to represent something useful (Bjornsson and Venegas, 1997).
389 Using this constraint, there are two modes $i=\{1,2\}$ that explain the variability in the 8-day AOD
390 measurements (see Figure 2). 38% of the variability in the AOD field maps to region $i = 1$ as shown
392 in Figure 2a, and which we will hence refer to as Northern Southeast Asia. 13% of the variability in
393 the AOD field maps to region $i=2$ as shown in Figure 2b, which we will hence refer to as Southern
394 Southeast Asia. The next largest mode contributes less than 5% to the total variance in the AOD
395 field, and therefore is indistinguishable from other sources of variability and error, such as non-

396 linear effects of El-Nino, planetary dynamical events such as the MJO, regional dynamical events,
397 small-scale perturbations, short-term anthropogenic events, un-accounted for variations in cloud-
398 cover, bias in the data, new urbanization around the edges of the growing megacities, and such.

399 The physical relevance of these mathematical modes is established by correlating the
400 computed measured average AOD over the respective regions S_i , as a time series, with the
401 respective Principal Component T_i . The modes are found to be highly correlated with both the AOD
402 over Northern Southeast Asia ($R^2=0.86$, $p<0.01$) and the AOD over Southern Southeast Asia
403 ($R^2=0.86$, $p<0.01$), as shown in Figures 2c and 2d.

404 Over Northern Southeast Asia there is a partially bi-annual peak, with some years having a
405 single peak and others have two peaks. The major peak, which is the more pronounced or sole peak,
406 occurs every year in the measured AOD averaged over T_1 during the latter part of the local dry
407 season (from mid-February to late-April). Looking at the average value of the time series of the
408 AOD measurements over S_1 , it is found that the AOD peaks at the same time as T_1 peaks, and that
409 the average AOD ranges from 0.46 to 0.86, depending on the year. The smaller peak occurs in
410 August and September as shown in T_1 in most of the years (but not in 2008, 2010, and 2011).
411 Similarly, the average of the measured AOD over the region S_1 during the same months and years
412 has a corresponding peak ranging from 0.40 to 0.63 during the years when the second peak occurs.
413 The only disagreement between T_1 and the measured time series of averaged AOD over S_1 occurs
414 during 2003, which has already been noted previously by (Cohen, 2014), although none of the
415 variables used in this study can explain why.

416 Over Southern Southeast Asia, there is a one-to-one agreement between the peaks in T_2 and
417 the peaks in the averaged measurements of AOD over S_2 , with the peaks occurring in 6 years
418 (2001, 2002, 2004, 2006, 2009, and 2012) and not occurring in the other 7 years. The measured
419 peak in the average AOD ranges from 0.5 to 1.2, indicating that when these events occur, their
420 impact on the aerosol loading is larger than in Northern Southeast Asia. The timing of the peaks is

421 also wider and less well constrained than in Northern Southeast Asia, corresponding to most of the
422 entire dry season, from early-August to the end of October. Furthermore, there is no observed
423 second or smaller peak.

424 However, the issue of cloud cover leading to missed positives is observed in Southern
425 Southeast Asia. While this method was able to pick up the high haze and pollution years of 2002,
426 2004, the El-Nino in 2006, and 2009, two additional high haze and pollution years of 2010 and
427 2013 were not captured. As already shown in (Cohen, 2014), which was capable of capturing 2010
428 and 2013, the likely cause is cloud cover. We have confirmed that the MODIS cloud cover is in fact
429 the culprit, with there being fewer than 10% of pixels containing measurements of AOD over the
430 regions given by **S2**. In fact, the only time during these years that the results are found for these
431 years is in S_i where i is greater than 2, and thus are under the threshold used for statistical
432 robustness. This reconfirms the afore mentioned results that MISR is in fact better at dealing with
433 cloudiness over this region.

434 Careful consideration of **T1** (see Figure 2c) shows that it is considerably more noisy than **T2**
435 (see Figure 2c), and there are three explanations for this. First is because part because the emissions
436 from the region are more complex. In addition to the fires, there are large urban sources from three
437 megacities: Bangkok, Ho Chi Minh City, Hanoi, as well as many highly populated and inhabited
438 areas outside of these cities throughout the countryside. The emissions from these cities is
439 consistent throughout the year, and therefore the high frequency noise in these emissions, such as
440 day/night differences, weekday/weekend differences, etc. tends to make the signal slightly more
441 noisy. Secondly is that the fires in this region are due to combination of a few factors, which occur
442 on different scales and have various different size holdings in each case, meaning that small
443 differences in timing, intensity, and duration are to be expected from when the people decide to
444 burn and how long they decide to burn for (Taylor, 2010). There is agricultural/straw burning in
445 Thailand, subsistence burning in Cambodia, forest clearing in Myanmar and Laos, and urban and

446 agricultural expansion in Vietnam, with some of these agricultural regions, especially related to rice,
447 have 2 crops a year, and hence the possibility of being burned more than once (Dennis, 2005;
448 Tipayarom and Oanh, 2007). Thirdly, the dry season here tends to be extremely dry, without even
449 occasional rainstorms. Therefore, any emitted particles tend to have a very long lifetime. Hence, the
450 impact of secondary chemistry is important. This chemistry tends to be very sensitive to the
451 emissions ratios, to clouds, and to any non-linearly emitted secondary species from urban areas as
452 the plums proceeds downwind. On the other hand, in Southern Southeast Asia, the population is
453 also large, but in many of the places in Indonesia and Malaysia that are source regions, the cities are
454 large and well contained, while the countryside is still relatively empty. Secondly, in this region, the
455 major cause of burning is the clearing of primary forests, and much of this is done by a smaller
456 number of large-land holders, further reducing the variability. This is especially so on a year-to-year
457 basis, during some years which there is relatively little burning at all. Finally, even during the dry
458 season, there is still a considerable amount of small scale convective precipitation and day/night
459 sea/land breezes and rain. Hence, the lifetime of the particles and secondary precursors tends to be
460 slightly shorter, and the impacts of non-linear secondary processing is also reduced. Hence, the fact
461 that Southern Southeast Asia often has an even higher average AOD, means that the emissions must
462 be considerably larger in terms of magnitude from year to year, although not necessarily more
463 variable within each year, as also found in (Cohen, 2014).

464 These results are clearly consistent with the time-averaged values of the land-use
465 measurements of LAI and NDVI when averaged over regions **S1** and **S2** respectively (Figure 2).
466 Over **S1**, we can clearly see that much of the region either has an average LAI which is far too low
467 to correspond to native of secondary forest, implying that the land is now agriculture. In other cases,
468 there is still a high average LAI value with a corresponding reduction in NDVI, implying that
469 primary forest is being deforested in exchange for some type of commercial agricultural tree crop,
470 such as palm oil, rubber, or wood for paper. However, the region over which this second category is

471 occurring is smaller in size than the first region with the simultaneous decrease in both LAI and
472 NDVI (Huete et al., 2002; Myneni et al., 2002, 2007). On the other hand, over the region S2 we find
473 that the LAI is still generally quite high throughout the region of interest, while the average NDVI
474 is falling at an even faster rate than the drop over the smaller region in S1 in which a similar type of
475 condition is occurring. This is completely consistent with the known large-scale deforestation
476 occurring throughout Indonesia and Malaysia where mostly primary forest is burned and replaced
477 with large-scale agricultural tree-based crops (Dennis, 2005; Phillips et al., 2010; Taylor, 2010;
478 Wooster et al., 2012; Field et al., 2009).

479 A spatial mapping of the climatological mean and standard deviations of LAI and NDVI
480 over Southeastern Asia are displayed in Figure 3. First, it is observed that the LAI is smaller in
481 average over Northern Southeast Asia (LAI=2.3) then over Southern Southeast Asia (LAI=3.5).
482 Similarly for NDVI, the average value over Northern Southeast Asia is (NDVI=0.61) while it over
483 Southern Southeast Asia it is (NDVI=0.70). This is consistent with the knowledge that in Northern
484 Southeast Asia, the land has been more altered from its base tropical rainforest state (Natalia Hasler
485 and Avissar, 2009; Taylor, 2010). In fact, there is a considerable amount of rice and other agriculture
486 which has completely replaced trees with crops. Also, the pace of forest clearing is quite rapid in
487 those regions which still retain a considerable amount of native forest. The only considerably
488 widespread regions of native forests are left only in Laos and and at the frontier regions near the
489 intersection of Laos, Thailand, and Myanmar.

490

491 **3.2 Influence of Measured Fires**

492 To look at the impacts of measured fires, we fit the relationships between LAI, NDVI,
493 Precipitation and AOD in two cases, both with and without the inclusion of the Fire Count variable
494 using REG1 and REG2. This is done separately over both the Northern and Southern regions with
495 the corresponding different thresholds. A comparison of the time series of the region averaged AOD

496 from each EOF region, the 4 model predicted AOD values, and the measured averaged AOD is
497 made. The average statistical error and average statistical correlation (coefficient of determination,
498 R^2) between the datasets and the regression-fit model predicted AOD used to determine which
499 threshold τ is ultimately used for the purpose of determining the best fit coefficients for α_i , β_i , γ_i ,
500 and δ_i . The resulting statistics are displayed in Table 1.

501 As expected, including the Fire Count variable significantly increases the performance of
502 the algorithm in terms of correlations: on average the correlation increases from 70% to 79% in the
503 Northern region, and from 66% to 75% in the Southern region. However, there is no improvement
504 in the mean error between the reconstructed data and the original measured AOD. This means that if
505 there is a hotspot measurement available, it will improve the ability to predict the spatial and
506 temporal distribution of the fires, but provides no help in terms of estimating the AOD or emissions.
507 This is physically consistent, since the actual emissions should be a more complex function of the
508 type of burning, the material burned, and the conditions under it was burned, not just the existence
509 of a fire. Additionally, this is consistent because the Fire Count product only quantifies the
510 likelihood of a fire occurring within the given pixel, but provides no information on the intensity of
511 the fire. Furthermore, the results of the fitting of the regression coefficient associated to Fire Count
512 (Figure 4) show that the coefficient is strongly positive over the regions where fire are the most
513 important and AOD variability the strongest (regions within the dots). Thus, the results are found to
514 be consistent with what is understood, that Fire Count is a reasonable predictor of emissions of
515 aerosols from fires, but that this factor is only useful as a predictor of the effect, not as a means of
516 understanding the magnitude of the effect.

517 The best fit regression coefficients associated with NDVI make more physical sense in the
518 case where the Fire Count predictor is used REG1 (Figure A2a) than in the case where it is not
519 REG2 (Figure A2b). In all cases, the timing is based on the 8-day period in the year, from day 1 to 8
520 being the first data point, from day 9 to 16 being the second data point, etc. In this way, multi-year

521 variances in the climatology can be rigorously analyzed. In general a negative coefficient is found,
522 which implies that regions will lose NDVI as a result of an increase in AOD, which is consistent
523 with the health of the land decreasing during a fire. A similar gain is also found in terms of the best
524 fit coefficients for LAI in the regions which are not rice dominant (rice has a significantly low LAI
525 so that the signal to noise ratio from the satellite product is too low to produce a statistically
526 significant result over these regions). The regression coefficients are thus consistent and for this
527 reason, we only refer to REG1 from this point forward.

528 Making comparisons between the regression constructed AOD and the measured
529 AODMODIS over Northern Southeast Asia leads to the determination that in average, using τ_{North}
530 = P75(PC1) as the threshold of fire activity leads to the best results, as shown in Table 1. This leads
531 to the reasonable conclusion that in order to represent the AOD during the fire season well, there
532 must be greater access to data, while to represent the AOD during the non-burning or low-burning
533 seasons, that less data is required. This is consistent with the variability being considerably larger
534 during the burning season in both space and time over the region of interest.

535 On the other hand, for Southern Southeast Asia, using a very small value of τ_{South} =
536 P12.5(PC2) gives the best statistics. This means that using less data improves the fit during the fire
537 season as compared to the use of more data which better constrains the fit over the whole year. This
538 is not intuitive and is only consistent with the case that either (a) the data is more likely to be of low
539 quality during the burning season (i.e. the data is corrupted by clouds), or that there is a
540 considerable amount of data missing during the burning season (which is also possible due to the
541 widespread distribution of clouds over much of both Borneo and Sumatra). This view is also
542 consistent with the year-to-year and decadal scale of variability, wherein some years will have little
543 to no fire, and hence data is required over a considerably longer period of time, including both high-
544 and low-fire years in order to properly reproduce the observed patterns. For the remaining of this
545 analysis, we only consider (1) that the reconstructed data set of AOD over the Northern region has

546 been computed by using $\tau_{\text{North}} = P75(\text{PC1})$ as fire threshold, and (2) that the reconstructed data set
547 of AOD over the Southern region has been computed by using $\tau_{\text{South}} = P12.5(\text{PC2})$ as fire
548 threshold. These two data sets will be referred as AODNorth,REC and AODSouth,REC.

549

550 **3.3 Comparing AERONET measurements over Northern Southeast Asia**

551 Seven stations from AERONET are situated within the Northern region (Chiang Mai, Pimai,
552 Bac Giang, Nghia Do, Vientiane, Mukdahan, and Ubon Ratchathani) and four stations are located
553 inside the Southern region (Jambi, Kuching, Palangkaraya, and Singapore). The location of those
554 stations is displayed in Figure 3 and Table D. Of these stations, three are urban sites located
555 downwind from burning regions: Singapore, Bac Giang and Nghia Do, while the remaining sites are
556 located directly in or adjacent to burning areas. Figure 5 displays the temporal series of the
557 AERONET AOD (black curve) and regression-fit modeled AOD (blue curve) at the seven stations
558 situated within the Northern region. Table 4 displays the statistics of the goodness of fit between the
559 measured AOD and the reconstructed AOD respectively, AODMODIS and AODNorth, in terms of
560 reproducing the AERONET measured AOD signal.

561 The first general observation is that all AERONET stations in Northern Southeast Asia have
562 an annual peak in their AOD which occurs during the fire season, from February through April each
563 year. Additionally, each station has a smaller second peak over many of the years, but not annually,
564 occurring in August or September. At the two remote stations: Pimai (Figure 5c) and Ubon
565 Ratchathani (Figure 5d), AOD reaches its maximum value of over 0.5 during the fire season, while
566 generally the values are clean throughout the rest of the year except for 2001 to 2006, and 2009,
567 with a second local maximum of around 0.46 in September and October. At Pimai, the AERONET
568 data shows high pollution during the fire season every year from 2003 to 2008. The model captures
569 all these events correctly in terms of duration, with the onset and end times slightly off, leading to a
570 correlation of 43%, with an intensity mean error of -0.12. At Ubon Ratchathani, the AERONET data

571 shows high pollution events during the fire season of the years 2010 to 2012. The model captures all
572 these events in terms of duration (correlation of 80%) but underestimates the intensity by a slightly
573 larger mean error of -0.22. A large peak of high AOD can be seen in September 2012
574 corresponding to a high-pollution event also observed in Singapore. This peak, which has a
575 maximum AOD value of 0.6, is captured by the model. During the common years of data between
576 AERONET and AODNorth (2008 to 2013), we calculate that the model captures the fire season and
577 the pollution that is generated by it in terms of duration (correlation is 64%) and less well in terms of
578 intensity (mean error of -0.26). Although the error in the intensity is not insignificant, it is still
579 significantly better than most other errors from model studies over heavily biomass burning
580 influenced areas of the world, the mean error is still quite good, since most admit to requiring a
581 scaling factor from 1.7 to as much as 5 (e.g.: Wu et al., 2011; Cohen and Wang, 2014; Hodnebrog et
582 al., 2014).

583 There are three stations which are situated at medium-sized urban sites which are also
584 adjacent to or directly upwind from fire burning regions: Chiang Mai, (Figure 5e), Mukdahan
585 (Figure 5f), and Vientiane (Figure 5g). All show a strong annual peak during the fire season from
586 February to April. At Chiang Mai and Mukdahan, which are nearer to the agricultural fires, the
587 maximum value of AOD is around 0.5, while it is around 0.6 at Vientiane, which is located further
588 downwind and hence able to undergo additional secondary processing. Figures 5e, 5f, and 5g also
589 show smaller peaks during other parts of the year: from September to October for the years 2001 to
590 2006 at Chiang Mai, with a maximum AOD value of 0.4; from July/August and to October/
591 November (depending on the years) for the years 2001 to 2007, 2009, and 2010 at Mukdahan, with
592 a maximum AOD value of 0.44; and from September to October for the years 2001 to 2007, and
593 2009 at Vientiane, with a maximum AOD value of 0.59. The nature of these secondary peaks are
594 not annual in occurrence. At Mukdahan, the AERONET data demonstrates the fire season peak for
595 every year the data exists: 2004, 2006, 2007, 2008, and 2009. The regression-fit model reproduces

606 the high pollution every year ($R^2=0.69$), while also reproducing the intensity correctly in 2007 and
607 2009. While there is only very sparse AERONET data at Vientiane, the regression-fit model
608 reproduces the signal well ($R^2=0.64$ and $RMS=-0.07$) (see Table 4). Finally, the model also captures
609 the high pollution events measured in March, April, and September 2012.

600 As expected, there is a considerable amount of variability at stations which are in or near
601 large urban areas (Megacities), due to the combination of both the fire signal as well as local
602 emissions and in-situ secondary processing. In particular, the signals at the two stations near to the
603 rapidly growing urban megacity of Hanoi: Bac Giang (Figure 5a) and Nghia Do (Figure 5b) are
604 very similar. These stations have a much higher annual average AOD than the other stations in the
605 region, with the daily average value as well as long-term mean measured AOD being frequently
606 larger than 0.4, while the annual high AOD peak has a yearly maximum of at least 0.9 at both of
607 these stations (see Table 3). Figures 5a and 5b also show smaller AOD peaks (maximum value of
608 around 0.7) during other parts of the year (from July through November depending on the year).
609 During the fire seasons in 2004 and 2007 at Bac Giang, the timing of the high pollution events are
610 well-captured by the regression-fit model, in terms of onset, duration, and end time, although the
611 model intensity is underestimated.

612 In 2006, the Southern Southeast Asian fire season produced an extensive and massive
613 amount of emissions T2 due to extremely dry and warm conditions brought on by the El-Nino
614 conditions. Various models and measurements have shown that the fires from these emissions have
615 spread from S2 throughout the Indian and Pacific Oceans (Podgorny et al., 2003). However, we
616 have also found that the signal is clearly present at all of the stations located in S1. At Chiang Mai,
617 Mukdahan, and Pimai both the intensity of the 2006 season as well as its onset, duration, and
618 conclusion are all well reproduced in both the AERONET measurements and the regression-fit
619 model. Even at the urban megacities Bac Giang and Nghia Do the AERONET measurements also
620 display a high pollution peak ($AOD=1.2$) around September 2006, while the regression models at

621 both of these stations capture the measured onset, duration, and ending of this event. The only issue
622 is that the magnitude of the regression-fit model AOD underestimates the measured value by as
623 much as 33% at Bac Giang.

624 Given the intimate connection between fires and the ensuing rapid changes of the land
625 surface which occur at the same time, as expected, LAI and NDVI have changed at the same
626 locations as the AERONET stations. First, they show a correspondingly higher value during the
627 second, localized peak, than at the major annual peak, with a maximum value of around 0.9 at these
628 stations (see Table 3). Figures 5a and 5b also show smaller AOD peaks (maximum value of around
629 0.7) during other parts of the year (July through November depending on the year), see Tables D
630 and 3. This is indicative that the second peak, which does not occur year- to-year, may not be
631 attributed to large-scale local burning, unless the local fires are much less extensive and thus do not
632 lead to significant change in the land surface, but happen to just be upwind of these measurement
633 stations in these given years, or that the local fires are much more polluting per unit of land use
634 change, and hence still contribute to the AOD to some extent. The other possible explanations are
635 that the pollution during these times is actually transported from other place, or are intensified due
636 to some sort of secondary processing. However, it is also found that these changes in the year-to-
637 year LAI and NDVI values do not vary in a one-to-one manner with T2, which has some covariance
638 during the big fire years of 2002, 2004, 2006, and 2009, but not during other years in which the
639 peak occurs, such as 2001, 2003, 2005, and 2007.

640 Overall, we find that the annual peak in AOD throughout **S1** is clearly due to fires, and that
641 this is true for both urban, partially urban, and remote sites. Further, during these fire events, the
642 dominant source contributing to the peak in AOD is from the burning itself, even in urban areas
643 where it may be one of two dominant sources. Additionally, there is a second peak found at these
644 stations, which is both smaller in magnitude, and only occurs in certain years. This secondary peak
645 is very likely not due to local burning, and instead it is shown that a significant number of these

646 years co-vary with analyzed large-scale fires from region **S2**, indicative of long-range transport.
647 However, since there are a few years during which this is also not the case, it is possible that other
648 sources of long-range transport or secondary production of aerosols, such as from South Asia.

649

650 **3.4 Comparing AERONET measurements over Southern Southeast Asia**

651 In Southern Southeast Asia, **S2**, the majority of the emissions come from a small number of
652 well-defined major urban centers, transport lines through the waterways, and wide-spread sources
653 from fires, with much of the region still continuing primary forest or dense secondary forest. As a
654 consequence, the major source of the variation in the AOD is a combination of the emissions from
655 fires and precipitation (as it is the major source of the aerosols removal from the atmosphere). This
656 is demonstrated in Figure 6, demonstrating a smoother and less variable set of measurements during
657 the wet season than at sites over Northern Southeast Asia, 5 and 6. Consequently, the AERONET
658 site in Singapore, the sole large urban area in **S2**, is very different from the other stations of this
659 subregion.

660 Unlike in Northern Southeast Asia, in general, the AOD signal in Southern Southeast Asia
661 tends to only peak once a year (except for in 2009 and 2014, which are special cases to be discussed
662 later that had 2 peaks due to primary fire emissions). This primary peak, as shown in **T2** always
663 occurs during the local fire season from August through October/November, without any additional
664 second peak occurring during a non-burning period, as in **T1**. Effectively, this implies that
665 emissions from **S1** are not contributing to the variance in the measured AOD over **S2** and that long-
666 range transport from Northern Southeast Asia is not efficient in contributing to the high peaks in
667 AOD found over **S2**.

668 Additionally, Southern Southeast Asia has an important source of uncertainty and bias in the
669 measurements over the region. Specifically, the impact of intense cloud cover is also determined to

670

671 be very important, in terms of being able to capture all of the known large-scale fire based events.
672 We observe that in a few special cases where known large-scale pollution events have occurred over
673 S2 as measured both on the ground and by MISR measurements of AOD (Cohen, 2014), that
674 MODIS was not able to successfully capture the events (for example: June 2013). A careful
675 examination of the cloud cover fields and Fire Count measurements show that this is clearly the
676 case, at least for June 2013; the region S2 was almost completely masked by clouds (over 80% of
677 all pixels) in the day-to-day tracks, with more than 90% of pixels in the 8-day average fields over
678 this period of time being masked.

679 The AERONET station in Singapore, is located in a highly urban environment, with
680 sizable sources of aerosol emissions related to shipping, a high energy using population, and
681 refineries. It is clear that there are no wild-fires occurring within Singapore. At the Singapore
682 station, we observe an annual signal except for every year, although during the years 2008 and
683 2010, the signal is less intense than in the other measured years. There is a considerable amount of
684 variation in the magnitude, the onset, and the duration of the peak, as well as a considerable amount
685 of noise. However, the maximum measured AOD here on an 8-day average basis, ranges from a low
686 year of 0.55 to a high year of 0.81 in 2006. Even though the fires were quite distant, it is clearly
687 observed that then most intense event in 2006 is readily captured here, further supporting that even
688 in an urban environment, Singapore offers a reasonable downwind signal site for observing the
689 impacts of the fires.

690 On the other hand, the other AERONET stations in this region, including in Kuching, Jambi,
691 and Palangkaraya, are situated in remote and mostly heavily jungle/forested regions of Borneo and
692 Sumatra islands (see Table D). These sites are all located close-by to where the fire sources
693 originate, in the jungles and forests of Borneo and Sumatra. The AERONET station in Jambi,
694 situated on Sumatra Island, has an annual signal of high AOD occurring once a year, every year,
695 except in 2010 (where there were no measurements). However, the magnitude, onset, and duration

696 of these high pollution events is highly variable from year to year. The AOD maximum value ranges
697 from a low of 0.67 (in 2007) to a high of 1.49 (in 2006) (see Table 5). The AERONET station in
698 Kuching has an annual peak signal in AOD every year that measurements are available (there were
699 no measurements during the corresponding peak times in 2008, 2010, and 2013). The magnitude,
700 start, and duration of this peak is again highly variable from year to year, with the maximum in
701 measured AOD ranging from a low of 0.68 in 2007 to a maximum of 1.36 in 2006. At
702 Palangkaraya, which is situated in Western Borneo in Indonesia, there is also a single high peak
703 occurring every year, except for 2010 (which did not have any measurements). Similar to the other
704 stations, the intensity, onset, and duration of the high AOD signal was very variable from year to
705 year.

706 The regressive-fit model based on the MODIS measurements at each of the remote sites in
707 Southern Southeast Asia: Jambi, Kuching, and Palangkaraya, is capable of reproducing the major
708 heavily polluted years as found in the measurements, such 2002 (max AOD of 1.24 in Jambi, 1.0 in
709 Kuching, and 1.94 in Palangkaraya), 2004 (max AOD of 0.99 in Jambi, 0.85 in Kuching, and 1.18
710 in Palangkaraya), 2006 (max AOD of 1.49 in Jambi, 1.4 in Kuching, and 1.98 in Palangkaraya),
711 and 2009 (max AOD of 0.95 in Jambi, 0.87 in Kuching, and 1.02 in Palangkaraya). At Jambi and
712 Palangkaraya, the regressive-fit model reproduces the high AOD event of late 2012 well, with a
713 better correlation with the AERONET measurements ($R^2=76\%$ at Jambi and $R^2=74\%$ at
714 Palangkaraya) than MODIS AOD at the same grid point ($R^2=51\%$ at Jambi and $R^2=71\%$ at
715 Palangkaraya), as given in Table 6, although the intensity in these years is slightly low. On the other
716 hand, the regressive-fit model reproduces the AOD well in terms of intensity, onset, and duration at
717 Kuching (RMS error of 0.13, $R^2=66\%$) (see Table 6). However, the regressive-fit model is still
718 basically constrained by the cloud cover issue. It is for this reason that the know high values of
719 aerosols in the atmosphere over Singapore in June of 2013 (as based on surface measurements and
720 personal observation) is not captured in AERONET measurements, MODIS measurements, or the

721 regressive-fit model. In addition to June 2013, we also find that MODIS AOD and the regressive fit
722 model are both not capable of capturing the 2010 fire season peak either. However, the issues of
723 cloud cover seem to be less important in other years, and we find the onset, duration, and intensity
724 are all well matched between the regressive-fit model and AERONET measurements at Singapore
725 during the fire seasons of the years 2007, 2008, 2009, 2011, and 2012 (see Table 6 for statistics).

726

727 **3.5 Comparisons versus measurements from the MISR satellite**

728 MISR satellite measurements of AOD are at lower spatial and temporal resolution than
729 MODIS and AERONET measurements, and thus to use them as a basis for comparison, the values
730 from MODIS and AERONET will be averaged to a monthly-basis as well as at $0.5^{\circ} \times 0.5^{\circ}$. Over
731 Northern Southeast Asia, the time series of the regression-fit model AOD compares very well with
732 the time series of the average MISR AOD over the same region ($R^2=0.77$ over **S1**, and $R^2=0.85$
733 over the region of highest variability). While there is some underestimation of the absolute AOD as
734 compared to the MISR measurements, that underestimation is always less than 0.1, and therefore is
735 not far from the order of magnitude of the error in the measurements themselves. One of the
736 important reasons why the agreement is so good is that this region is generally cloud-free during the
737 dry season when the fires occur, and hence there is a quite large and representatively similar
738 sampling size between MODIS, MISR, and AERONET during the fire periods in this region. This
739 establishes that indeed the MODIS based regression-fit model matches well against MISR, and is
740 able to reproduce the variability and magnitude of the AOD over Northern Southeast Asia (Figure
741 7).

742 Not surprisingly, when fitting the results of the MODIS regression-fit model using 8-day
743 average data, the overall fits are less good when comparing against MISR. Part of the issue is the
744 additional variability, but more importantly is the lack of sufficient data due to cloud coverage.
745 Specifically, over the region **S1**, the correlation rises from $R^2=0.66$ to $R^2=0.81$ when increasing

746 from 8-day to monthly averaging. Similarly, the comparison between the AERONET data and
747 MISR AOD also increases from $R^2=0.59$ to $R^2=0.79$ when comparing 8-day averages and monthly
748 averages respectively. Overall, the regression-fit model is able to reproduce the variation of AOD at
749 all the stations in Northern Southeast Asia, both in terms of duration and intensity concerning high
750 pollution events (see Figures B3 and B4).

751 As expected, the spatial comparison between MISR and the regression-fit model over
752 Southern Southeast Asia is less good. The first thing to note is that the spatial extent of the region
753 from MODIS, given with the relatively level of high certainty by S2, is considerably smaller than a
754 similar spatial distribution of the smoke extent over this same region, when analyzed in the same
755 way using data from MISR measurements (Cohen, 2014). This is explained in part due to the larger
756 cloud-covered fraction in the MODIS measurements when compared with MISR, as well as the
757 shorter averaging period with the MODIS measurements, leading to a situation where there is
758 insufficient information at each averaging time step over much of the region. It is found that the
759 RMS error between MISR and the regression-fit model ranges from a minor and relatively
760 insignificant (as compared to the measurement errors) model overestimate of 0.1 in AOD, to a
761 substantial and significant model underestimate in the AOD of up to 0.5. This regression-fit model
762 underestimates as compared to MISR measurements is significantly larger than the AERONET and
763 MISR disagreement over this region, which is less than 0.3 (Cohen, 2014; Shi et al., 2011) and
764 further, this error occurs especially and exclusively during the intense fire-burning years. On the
765 other hand, the overall temporal correlation between the regression-fit model and the time-average
766 AOD from MISR is $R^2=0.72$ over all and is as high as $R^2=0.79$ over the region of highest AOD
767 variability. This means that the inter-annual and intra-annual variation is relatively captured by the
768 MODIS measurements and the resulting regression-fit model.

769

770 4. Conclusions

771 An in-depth analysis of multiple measurements from MODIS, MISR, TRMM, and
772 AERONET measurements has been performed over a 13-year period over Southeast Asia. Using
773 MODIS AOD, the spatial and temporal patterns of the contribution of fires to the atmospheric
774 loading of aerosols was established. Two distinct regions, with vastly different properties were
775 observed: one in Northern Southeast Asia, which had a strong annual signal with some inter-annual
776 variability, and another in Southern Southeast Asia, which had a strong signal with inter-annual and
777 intra-annual variability. Northern Southeast Asia shows an annual high AOD during the fire season
778 (varying roughly from February through April), with a smaller nearly annual peak occurring during
779 the exact timing when Southern Southeast Asia has its fire season. Southern Southeast Asia is
780 affected every year by their own fires (from roughly August through October), without any
781 observed secondary peak except for during two exceptionally dry years during the second very short
782 dry season in February 2009 and the very end of 2013 (which would up maximizing in February
783 2014, although it is beyond the end of the data analyzed in this paper). The representation in terms
784 of the timing of the fires of Northern Southeast Asia was consistently good in terms of start time,
785 length of the burning season, cessation of the burning, when compared against AERONET and
786 MISR measurements. The representation in terms of timing over Southern Southeast Asia was not
787 as good, but still quite acceptable when compared against AERONET and MISR measurements,
788 with the duration of the fire season well captured in strong fire years, and the strongest part of the
789 fire season captured in low fire years.

790 Bringing in different simultaneous measurements of land-surface variables, fires,
791 precipitation, and column aerosol measurements, allows us to confirm that these patterns exist and
792 are consistent with land-use burning. Given the difference in the timing and durations of the major
793 monsoon seasons over these regions, the results are consistent. From this point, a simple regression-
794 fit model was established to predict the AOD from measurements of land-use change variables,
795 fires, and precipitation, which should be the basis upon which fires start in the environment. These

796 simple regression-fit models (based on MODIS and TRMM) reproduced the onset, duration, and
797 magnitude of the measured AOD from other measured sources (MISR and AERONET) well over
798 Northern Southeast Asia. The results of this regression-fit model demonstrate the ability to predict
799 the AOD as observed by AERONET and MISR, using only measurements of land-use change
800 variables and fires from MODIS, and precipitation from TRMM, measurements of some of the
801 important and fundamental underlying factors controlling the fires.

802 These simple regression-fit models reproduced the onset, duration, cessation, and even the
803 magnitude of the measured AOD from AERONET and MISR very well in Northern Southeast Asia.
804 These simple regression-fit models also reproduced the onset, duration, and cessation, of the
805 measured AOD from AERONET and MISR well well in Southern Southeast Asia, especially during
806 the more intense burning years. The main issue in Southern Southeast Asia, however, was that the
807 magnitude over this region was strongly underestimated. These results still underestimate the
808 column loading, but by a magnitude of 30% or less, which is far better than the typical scaling
809 factors applied of 1.7 (70%) or more, and consistent with the results in Cohen and Wang (2014) and
810 Cohen (2014) which show that there is an underestimate in both the overall magnitude as well as in
811 the fire magnitude, and that correcting for the former leads to an underestimate in the latter of 20%
812 to 30%. The result is not only larger in magnitude than the GFED emissions products, but include
813 regions which are considered to have zero emissions in the GFED data set, a worrying conclusion,
814 since a value of 0 cannot be scaled up by a scaling factor. Some reasons for this include emissions
815 sources which are more variable in space and time, such as the clearing of primary forests, peat
816 burning, and rapid development; and other limiting reasons such as increased cloud cover reducing
817 the number of available measurements over large portions of this region by a significant amount.
818 Further, the inter-seasonal periods in Southern Southeast Asia tend to be both more rainy and more
819 cloud-covered than in Northern Southeast Asia, due to large scale convection and other regional
820 disturbances like the MJO and the IOD.

821 There is a strong and consistent change in the land use variables occurring during the local
822 fire season over both Northern and Southern Southeast Asia, although these relationships, as
823 expected, are different over the two regions due to different types of land-use change. The
824 relationships between burning of primary forests, grasslands or crops, and peat should all be
825 different. Additionally, there is an important secondary use for these relationships, determining
826 whether the observed smoke is locally produced or transported from far upwind. For example, it is
827 clearly noted that the land-use changes are much smaller during the second non-annually occurring
828 peak in Northern Southeast Asia, implying that while there may be some contribution from local
829 sources, that there is also a large amount of smoke which is transported from other regions. This
830 comes from the idea that if the land itself did not change very much, then the emissions of smoke
831 produced must have been considerably lower. The timing of this smaller peak matches the timing of
832 the fire occurrence over Southern Southeast Asia with a very high level of correlation. Additionally,
833 it also cannot be ruled out that the smoke could be urban pollution from South Asia. On the other
834 hand, there is no evidence that any of the smoke in Southern Southeast Asia originates from any
835 region other than its own sources.

836 Further, we explored the added value of using higher temporal resolution data, which is
837 usually thought to add improved value. Due to the large amount of cloudiness encountered, there
838 was a much reduced number of measurements available over Southern Southeast Asia during the
839 fire season using 1-day average values as compared to 8-day average values, leading to less
840 statistical relevance. In the end, it was not possible to have a reasonable reproduction of the
841 measured AERONET and MISR values of the onset, duration, and ending of the fires using 1-day
842 average MODIS and TRMM data as compared to when using 8-day average MODIS and TRMM
843 measurements to develop the regression-fit relationships. Even with the 8-day average data and the
844 associated regression-fit relationships, the magnitude of AOD during Southern Southeast Asia's fire
845 season is significantly too low, although in Northern Southeast Asia, it is low but not more than the

846 magnitude of the uncertainty of the input measurements themselves. The correlation between the
847 regression-fit model AOD and AERONET stations over the entire decadal time period, using 8-day
848 average MODIS data, ranges from $R^2=0.42$ to $R^2=0.75$. While monthly-average data from MODIS
849 does not provide as fine resolution for the duration, onset, and end times of the fires, it provides the
850 best match in terms of the magnitude of the AOD measurements from AERONET and MISR.
851 However, when using MODIS data on a monthly average basis, the regression-fit model AOD gives
852 a better performance with the correlation coefficient between AOD and AERONET stations ranging
853 from $R^2=0.70$ to $R^2=0.90$. Furthermore, the correlation over the regions of interest S1 and S2
854 between the regression-fit model and MISR measurements of AOD ranges from $R^2=0.57$ to
855 $R^2=0.81$. This is due partially to less under-representation of very high short-term peaks, as well as
856 additional data points being available in the MODIS fire and land use products at longer average
857 time durations. This is a counter-intuitive result, with many in the community stressing the added
858 value of higher frequency measurements, but one which is consistent with the fact that such space-
859 born measurements are severely limited by clouds over this region of the world during the fire
860 season. MISR has shown to represent the magnitude of the AOD well, with the measurements from
861 monthly-average MISR measurements and monthly-average AERONET measurements being
862 basically the same. Therefore, the ability of the regression-fit model to capture the monthly-average
863 AOD from both MISR and AERONET, in terms of both the inter-annual and intra-annual variability
864 in the fire seasons, is significant, and shows that indeed the changes in the land surface and the
865 impacts of precipitation are what are driving the atmospheric loading of AOD and hence the impact
866 of the fires over this region on the decadal scale. Further, as it is widely known, peat can burn and
867 smolder for an extended period of time after any measured fire has gone away, and therefore, by
868 extending the average value for the fire, it allows for a better matching with the total emissions,
869 which will continue to often be produced for weeks after any visible flame or surface heat is
870 observed. Thusly, one of the important findings is to examine the most ideal temporal resolution at

871 which to use the data, whether it be daily, weekly, or monthly. While most of the published
872 literature leans towards using high frequency daily data (or individual swath-by-swath data, where
873 available), we determine and validate that using weekly or monthly average data leads to a better
874 ability to accurately reproduce the measured values, explain why that is the case, and then quantify
875 some of the impacts and limitations of this result.

876 This study highlights the importance of taking into account land-use variable and
877 precipitation for estimating AOD correctly both in time and magnitude, even if magnitude remains
878 hard to capture on a 8-day basis. One significant bias in the magnitude of the results must be due to
879 problems of the relationships over the region being not properly captured, such as the different
880 anthropogenic driving forces of the land-clearing being significantly different over the two regions.
881 A second significant bias in the magnitude is due to the fact that there is a significantly more cloud
882 cover over the two regions during their local burning seasons(Giglio et al., 2003). These results
883 support the efficacy of the approach introduced here: that it is appropriate to use measured changes
884 in the land, precipitation, and active fires from MODIS and TRMM to reproduce a working model
885 of the atmospheric aerosol loading. Furthermore, other than (Cohen, 2014; Cohen and Wang, 2014)
886 there are no other works that have been able to satisfactorily estimate the loadings of or AOD
887 associated with emissions aerosols over this region of the world, without using some type of
888 scaling. This method is able to reproduce the magnitudes by introducing physical parameterizations
889 of scaling, and doing so based on a more fundamental driver-based approach. This allows us to
890 improve our understanding of the relationships, both in terms of how they vary over space and time,
891 on one hand, and in terms of physical drivers, on the other.

892

893 **Acknowledgements**

894 This work was supported by the Young Thousand Talents Program of the Chinese National
895 Government, the Singapore National Research Foundation (NRF) through a grant to the Center for
896 Environmental Sensing and Monitoring (CENSAM) of the Singapore-MIT Alliance for Research
897 and Technology (SMART), and the Tropical Marine Sciences Institute. The authors also want to
898 thank all of the Principal Investigators of MISR, AERONET, NOAA, and MODIS, and TRMM for
899 making the data available.

900

References

- Afroz, R., Hassan, M. N., and Ibrahim, N. A.: Review of air pollution and health impacts in Malaysia, *Environmental research*, 92, 71–77, 2003.
- Aldrian, E., Gates, L. D., and Widodo, F.: Seasonal variability of Indonesian rainfall in ECHAM4 simulations and in the reanalyses: The role of ENSO, *Theoretical and Applied Climatology*, 87, 41–59, 2007.
- Asner, G. P., Scurlock, J. M., and A Hicke, J.: Global synthesis of leaf area index observations: implications for ecological and remote sensing studies, *Global Ecology and Biogeography*, 12, 191–205, 2003.
- Bjornsson, H. and Venegas, S.: A Manual for EOF and SVD Analyses of Climate Data. Department of Atmospheric and Oceanic Sciences and Centre for Climate and Global Change Research, Tech. rep., McGill University, Technical Report, 1997.
- Chang, C., Wang, Z., McBride, J., and Liu, C.-H.: Annual cycle of Southeast Asia-Maritime Continent rainfall and the asymmetric monsoon transition, *Journal of climate*, 18, 287–301, 2005.
- Chen, W., Wang, X., Cohen, J. B., Zhou, S., Zhang, Z., Chang, M., and Chan, C.-Y.: Properties of aerosols and formation mechanisms over southern China during the monsoon season, *Atmos. Chem. Phys.*, 16, 13271–13289, doi:10.5194/acp-16-13271-2016, 2016.
- Cohen, J. B.: Quantifying the occurrence and magnitude of the Southeast Asian fire climatology, *Environmental Research Letters*, 9, 114018, 2014.
- Cohen, J. B. and Prinn, R. G.: Development of a fast, urban chemistry metamodel for inclusion in global models, *Atmospheric Chemistry and Physics*, 11, 7629–7656, 2011.
- Cohen, J. B. and Wang, C.: Estimating global black carbon emissions using a top-down Kalman Filter approach, *Journal of Geophysical Research: Atmospheres*, 119, 307–323, 2014.
- Cohen, J. B., Prinn, R. G., and Wang, C.: The impact of detailed urban-scale processing on the composition, distribution, and radiative forcing of anthropogenic aerosols, *Geophysical Research Letters*, 38, 2011.
- Cuevas, G. M., Gerard, F., Balzter, H., Riano, D.: Analysing forest recovery after wildfire disturbance in boreal Siberia using remotely sensed vegetation indices, *Climate Change Biology*, Nov 3, 2008, 10.1111/j.1365-2486.2008.01784.x.
- Dennis, R.A., Grahame, J.M., Unna, A., Chokkalingam, U., Pierce, C.J., Kurniawan, I., Lachowski, H., Maus, P., Permana, R.P., Ruchiat, Y., Stolle, F., Suyanto, Tomich, T.P.: Fire, People and Pixels: Linking Social Science and Remote Sensing to Understand Underlying Causes and Impacts of Fires in Indonesia, *Human Ecology*, 33, 465–504, doi:10.1007/s10745-005-5156-z, <http://dx.doi.org/10.1007/s10745-005-5156-z>, 2005.
- Diner D J et al 1998 Multi-angle imaging spectroradiometer (MISR) instrument description and experiment overview *IEEE Trans. Geosci. Remote Sens.* 36 1072–87
- Dubovik, O., Smirnov, A., Holben, B., King, M., Kaufman, Y., Eck, T., and Slutsker, I.: Accuracy assessments of aerosol optical properties retrieved from Aerosol Robotic Network (AERONET) Sun and sky radiance measurements, *Journal of Geophysical Research: Atmospheres* (1984–2012), 105, 9791–9806, 2000.
- Field, R. D., van der Werf, G. R., and Shen, S. S.: Human amplification of drought-induced biomass burning in Indonesia since 1960, *Nature Geoscience*, 2, 185–188, 2009.
- Fisher, J. B., Malhi, Y., Bonal, D., Da Rocha, H. R., De Araujo, A. C., Gamo, M., Goulden, M. L., Hirano, T., Huete, A. R., Kondo, H., et al.: The land–atmosphere water flux in the tropics, *Global Change Biology*, 15, 2694–2714, 2009.

- Fu J S, Hsu N C, Gao Y, Huang K, Li C, Lin N-H and Tsay S-C 2012 Evaluating the influences of biomass burning during 2006 BASE-ASIA: a regional chemical transport modeling Atmos. Chem. Phys. 12 3837–55
- Fuller, D. and Murphy, K.: The Enso-Fire Dynamic in Insular Southeast Asia, *Climatic Change*, 74, 435–455, doi:10.1007/s10584-006-0432-5, <http://dx.doi.org/10.1007/s10584-006-0432-5>, 2006.
- Giglio, L., Desloîtres, J., Justice, C. O., and Kaufman, Y. J.: An enhanced contextual fire detection algorithm for MODIS, *Remote sensing of environment*, 87, 273–282, 2003.
- Giglio, L., Csiszar, I., and Justice, C. O.: Global distribution and seasonality of active fires as observed with the Terra and Aqua Moderate Resolution Imaging Spectroradiometer (MODIS) sensors, *Journal of Geophysical Research: Biogeosciences* (2005–2012), 111, 2006.
- Hansen, M. C., Stehman, S. V., Potapov, P. V., Loveland, T. R., Townshend, J. R., DeFries, R. S., Pittman, K. W., Arunarwati, B., Stolle, F., Steininger, M. K., et al.: Humid tropical forest clearing from 2000 to 2005 quantified by using multitemporal and multiresolution remotely sensed data, *Proceedings of the National Academy of Sciences*, 105, 9439–9444, 2008.
- Hodnebrog, O., Myhre, G., and Samset, B: How shorter black carbon lifetime alters its climate effect. *Nature Communications* 5, Article number: 5065 (2014) doi:10.1038/ncomms6065.
- Holben, B., Eck, T., Slutsker, I., Tanre, D., Buis, J., Setzer, A., Vermote, E., Reagan, J., Kaufman, Y., Nakajima, T., et al.: AERONET: A federated instrument network and data archive for aerosol characterization, *Remote sensing of environment*, 66, 1–16, 1998.
- Huang, J., Minnis, P., Lin, B., Wang, T., Yi, Y., Hu, Y., Sun-Mack, S., and Ayers, K.: Possible influences of Asian dust aerosols on cloud properties and radiative forcing observed from MODIS and CERES, *Geophysical Research Letters*, 33, 2006.
- Huete, A., Justice, C., and Van Leeuwen, W.: MODIS vegetation index (MOD13), Algorithm theoretical basis document, 3, 213, 1999.
- Huete, A., Didan, K., Miura, T., Rodriguez, E. P., Gao, X., and Ferreira, L. G.: Overview of the radiometric and biophysical performance of the MODIS vegetation indices, *Remote sensing of environment*, 83, 195–213, 2002.
- Jacobson, M. Z.: Strong radiative heating due to the mixing state of black carbon in atmospheric aerosols, *Nature*, 409, 695–697, 2001.
- Kahn R. A., B. J. Gaitley, M. J. Garay, D. J. Diner, T. F. Eck, A. Smirnov, and B. N. Holben (2010), Multiangle Imaging SpectroRadiometer global aerosol product assessment by comparison with the Aerosol Robotic Network, *J. Geophys. Res.*, 115, D23209, doi:10.1029/2010JD014601.
- Langmann, B., Duncan, B., Textor, C., Trentmann, J., and van der Werf, G. R.: Vegetation fire emissions and their impact on air pollution and climate, *Atmospheric Environment*, 43, 107–116, 2009.
- Levy, R. C., Mattoo, S., Munchak, L. A., Remer, L. A., Sayer, A. M., Patadia, F., and Hsu, N. C.: The Collection 6 MODIS aerosol products over land and ocean, *Atmos. Meas. Tech.*, 6, 2989–3034, doi:10.5194/amt-6-2989-2013, 2013.
- Lin, C.-Y., Hsu, H.-m., Lee, Y. H., Kuo, C. H., Sheng, Y.-F., and Chu, D. A.: A new transport mechanism of biomass burning from Indochina as identified by modeling studies, *Atmos. Chem. Phys.*, 9, 7901–7911, doi:10.5194/acp-9-7901-2009, 2009.
- Lin, C.-Y., Zhao, C, Xiaohong, L., Lin, N.-H., and Chen, W.: Modelling of Long-Range Transport of Southeast Asia Biomass-Burning Aerosols to Taiwan and their Radiative Forcings over East Asia, *Tellus B*, 2014, 66, 23733, <http://dx.doi.org/10.3402/tellusb.v66.23733>.
- Miettinen, J., Hyer, E., Chia, A. S., Kwoh, L. K., and Liew, S. C.: Detection of vegetation fires and burnt areas by remote sensing in insular Southeast Asian conditions: current status of knowledge and future challenges, *International Journal of Remote Sensing*, 34, 4344–4366, 2013.

- Ming, Y., Ramaswamy, V., and Persad, G.: Two opposing effects of absorbing aerosols on global-mean precipitation, *Geophysical Research Letters*, 37, 2010.
- Morawitz, D. F., Blewett, T. M., Cohen, A., and Alberti, M.: Using NDVI to Assess Vegetative Land Cover Change In Central Puget Sound, *Environmental Monitoring and Assessment* (2006) 114: 85–106.
- Myneni, R., Hoffman, S., Knyazikhin, Y., Privette, J., Glassy, J., Tian, Y., Wang, Y., Song, X., Zhang, Y., Smith, G., et al.: Global products of vegetation leaf area and fraction absorbed PAR from year one of MODIS data, *Remote sensing of environment*, 83, 214–231, 2002.
- Myneni, R. B., Yang, W., Nemani, R. R., Huete, A. R., Dickinson, R. E., Knyazikhin, Y., Didan, K., Fu, R., Juárez, R. I. N., Saatchi, S. S., et al.: Large seasonal swings in leaf area of Amazon rainforests, *Proceedings of the National Academy of Sciences*, 104, 4820–4823, 2007.
- Nakajima, T., Higurashi, A., Takeuchi, N., and Herman, J. R.: Satellite and ground-based study of optical properties of 1997 Indonesian Forest Fire aerosols, *Geophysical Research Letters*, 26, 2421–2424, 1999.
- Natalia Hasler, D. W. and Avissar, R.: Effects of tropical deforestation on global hydroclimate: a multimodel ensemble analysis, *J. Climate*, 22, 1124–1141, doi:10.1175/2008JCLI2157.1, 2009.
- Neale, R. and Slingo, J.: The maritime continent and its role in the global climate: A GCM study, *Journal of Climate*, 16, 834–848, 2003.
- Nightingale, J., Nickeson, J., Justice, C., Baret, F., Garrigues, S., Wolfe, R., et al.: Global validation of EOS land products, lessons learned and future challenges: A MODIS case study, in: Available from. *Proceedings of 33rd International Symposium on Remote Sensing of Environment: Sustaining the Millennium Development Goals*, Stresa, Italy. http://landval.gsfc.nasa.gov/pdf/ISRSE_Nightingale.pdf, p. 4, 2008.
- Hope, A., Tague, C., and Clark, R.: Characterizing post-fire vegetation recovery of California chaparral using TM/ETM+ time-series data: *International Journal of Remote Sensing* 28, 6, 2007. <http://dx.doi.org/10.1080/01431160600908924>.
- Petrenko, M. and Ichoku, C.: Coherent uncertainty analysis of aerosol measurements from multiple satellite sensors, *Atmos. Chem. Phys.*, 13, 6777–6805, doi:10.5194/acp-13-6777-2013, 2013.
- Petrenko, M., Kahn, R., Chin, M., Soja, A., Kucsera, T., et al.: The use of satellite-measured aerosol optical depth to constrain biomass burning emissions source strength in the global model GOCART, *Journal of Geophysical Research: Atmospheres* (1984–2012), 117, 2012.
- Phillips, O. L., Van der Heijden, G., Lewis, S. L., López-González, G., Aragão, L. E., Lloyd, J., Malhi, Y., Monteagudo, A., Almeida, S., Dávila, E. A., et al.: Drought–mortality relationships for tropical forests, *New Phytologist*, 187, 631–646, 2010.
- Podgorny, I., Li, F., and Ramanathan, V.: Large aerosol radiative forcing due to the 1997 Indonesian forest fire, *Geophysical Research Letters*, 30, 2003.
- Ramanathan, V. and Carmichael, G.: Global and regional climate changes due to black carbon, *Nature geoscience*, 1, 221–227, 2008.
- Reid, J. S., Hyer, E. J., Johnson, R. S., Holben, B. N., Yokelson, R. J., Zhang, J., Campbell, J. R., Christopher, S. A., Di Girolamo, L., Giglio, L., et al.: Observing and understanding the Southeast Asian aerosol system by remote sensing: An initial review and analysis for the Seven Southeast Asian Studies (7SEAS) program, *Atmospheric Research*, 122, 403–468, 2013.
- Remer, L. A., Mattoo, S., Levy, R. C., and Munchak, L. A.: MODIS 3 km aerosol product: algorithm and global perspective, *Atmospheric Measurement Techniques*, 6, 1829–1844, doi: 10.5194/amt-6-1829-2013, <http://www.atmos-meas-tech.net/6/1829/2013/>, 2013.
- Rosenfeld, D.: TRMM observed first direct evidence of smoke from forest fires inhibiting rainfall, *Geophysical Research Letters*, 26, 3105–3108, 1999.

- Saatchi, S., Asefi-Najafabady, S., Malhi, Y., Aragao, L., Anderson, L., Myneni, R., and Nemani, R.: Persistent effects of a severe drought on Amazonian forest canopy, *PNAS*, January 8, 2013, 110, 2, p565–570.
- Sayer, A. M., Smirnov, A., Hsu, N. C., Munchak, L. A., and Holben, B. N.: Estimating marine aerosol particle volume and number from Maritime Aerosol Network data, *Atmos. Chem. Phys.*, 12, 8889–8909, doi:10.5194/acp-12-8889-2012, 2012.
- Shi, Y., Zhang, J., Reid, J. S., Hyer, E. J., Eck, T. F., Holben, B. N., and Kahn, R. A.: A critical examination of spatial biases between MODIS and MISR aerosol products; application for potential AERONET deployment, *Atmospheric Measurement Techniques*, 4, 2823–2836, doi: 10.5194/amt-4-2823-2011, <http://www.atmos-meas-tech.net/4/2823/2011/>, 2011.
- Tao, W.-K., Chen, J.-P., Li, Z., Wang, C., and Zhang, C.: Impact of aerosols on convective clouds and precipitation, *Reviews of Geophysics*, 50, 2012.
- Taylor, D.: Biomass burning, humans and climate change in Southeast Asia, *Biodiversity and Conservation*, 19, 1025–1042, doi:10.1007/s10531-009-9756-6, <http://dx.doi.org/10.1007/s10531-009-9756-6>, 2010.
- Tipayarom, D. and Oanh, N. K.: Effects from open rice straw burning emission on air quality in the Bangkok Metropolitan Region, *Science Asia*, 33, 339–345, 2007.
- van der Werf, G. R., Randerson, J. T., Giglio, L., Collatz, G. J., Kasibhatla, P. S., and Arellano Jr, A. F.: Interannual variability in global biomass burning emissions from 1997 to 2004, *Atmospheric Chemistry and Physics*, 6, 3423–3441, 2006.
- van der Werf, G. R., Dempewolf, J., Trigg, S. N., Randerson, J. T., Kasibhatla, P. S., Giglio, L., Murdiyarso, D., Peters, W., Morton, D. C., Collatz, G. J., Dolman, A. J., and DeFries, R. S.: Climate regulation of fire emissions and deforestation in equatorial Asia, *Proceedings of the National Academy of Sciences*, 105, 20350–20355, doi:10.1073/pnas.0803375105, <http://www.pnas.org/content/105/51/20350.abstract>, 2008.
- Wang, C.: Impact of direct radiative forcing of black carbon aerosols on tropical convective precipitation, *Geophysical research letters*, 34, 2007.
- Wang, C.: Impact of anthropogenic absorbing aerosols on clouds and precipitation: A review of recent progresses, *Atmospheric Research*, 122, 237–249, 2013.
- Wohl, E., Barros, A., Brunzell, N., Chappell, N. A., Coe, M., Giambelluca, T., Goldsmith, S., Harmon, R., Hendrickx, J. M., Juvik, J., et al.: The hydrology of the humid tropics, *Nature Climate Change*, 2, 655–662, 2012.
- Wooster, M. J., Perry, G. L. W., and Zoumas, A.: Fire, drought and El Niño relationships on Borneo (Southeast Asia) in the pre-MODIS era (1980–2000), *Biogeosciences*, 9, 317–340, doi:10.5194/bg-9-317-2012, <http://www.biogeosciences.net/9/317/2012/>, 2012.
- Wu, L., H. Su, and J. H. Jiang (2011), Regional simulations of deep convection and biomass burning over South America: 1. Model evaluations using multiple satellite data sets, *J. Geophys. Res.*, 116, D17208, doi:10.1029/2011JD016105.
- Yang, W., Tan, B., Huang, D., Rautiainen, M., Shabanov, N. V., Wang, Y., Privette, J. L., Huemmrich, K. F., Fensholt, R., Sandholt, I., et al.: MODIS leafareaindex products: From validation to algorithm improvement, *Geoscience and Remote Sensing, IEEE Transactions on*, 44, 1885–1898, 2006.
- Zhou S.Z., Perry K.D., Wang, X., Cohen, J.B., Liang, J., Huang, M., Fan, Q., Chen, W., Chang, M., Ancelet, T., and Trompeter, W.J.: High time-resolved elemental components in fine and coarse particles in the Pearl River Delta region of Southern China: Dynamic variations and effects of meteorology. *Science of the Total Environment*, <http://dx.doi.org/10.1016/j.scitotenv.2016.05.194>, 2016.

Table 1. Average error and correlation between AOD at 0.55 microns from MODIS and reconstructed AOD with different thresholds : $\tau = P90(PC)$, $\tau = P87.5(PC)$, $\tau = P83.5(PC)$, and $\tau = P75(PC)$ on the Northern and Southern regions, obtained by using REG1 and REG2.

Region	t = P90(PC)	t = P87:5(PC)	t = P83:5(PC)	t = P75(PC)
	Err/Corr(%)	Err/Corr(%)	Err/Corr(%)	Err/Corr(%)
North (w/ Fire Count)	-0.02/76	-0.02/78	-0.02/80	-0.01/83
North (w/o Fire Count)	-0.02/69	-0.02/70	-0.02/71	-0.02/71
South (w Fire Count)	-0.01/77	-0.01/78	-0.01/75	0.01/69
South (w/o Fire Count)	-0.01/71	-0.01/70	-0.01/66	-0.01/57

Table 2. Statistics over the respective Northern and Southern regions compared to the AERONET stations. Overlapped periods between the reconstructed AOD AOD_{North}/South and AERONET are stated in parenthesis. Fire denotes data analyzed only during the fire season, while All denotes the entire data set.

Stations	AOD _{MODIS}	AOD _{North}	AOD _{South}
	Err/Corr (%)	Err/Corr (%)	
Chiang Mai All (218/598)	-0.1/83	-0.1/75	
Bac Giang All (154/598)	-0.03/74	-0.06/42	
Mukdahan All (238/598)	-0.01/79	-0.01/69	
Nghia Do All (79/598)	-0.12/74	-0.14/42	
Pimai All (120/598)	0.0/77	-0.01/57	
Ubon Ratchathani All (99/598)	-0.01/88	-0.02/61	
Vientiane All (36/598)	-0.08/83	-0.07/64	
Chiang Mai Fire (62/151)	-0.26/91	-0.26/64	
Bac Giang Fire (46/151)	-0.07/75	-0.24/33	
Mukdahan Fire (74/151)	-0.08/86	-0.15/49	
Nghia Do Fire (15/151)	-0.08/75	-0.5/62	
Pimai Fire (45/151)	-0.03/75	-0.12/43	
Ubon Ratchathani Fire (23/151)	-0.07/88	-0.22/80	
Vientiane Fire (8/151)	-0.14/93	-0.33/92	
Jambi All (64/598)	-0.12/51		-0.26/76
Kuching All (91/598)	0.06/75		0.13/66
Palangkaraya All (65/598)	-0.11/71		-0.11/74
Singapore All (279/598)	-0.02/29		0.01/44
Jambi Fire (6/74)	-0.51/80*		-0.54/71*
Kuching Fire (10/74)	-0.28/80		-0.03/-9*
Palangkaraya Fire (6/74)	-0.5/85		-0.45/31*
Singapore Fire (24/74)	-0.23/-21*		-0.09/8*

* not statistically significant at the $p = 0.05$ level.

Table 3. Average values of maximum AOD and average LAI and NDVI during the two annual AOD peaks over the Northern region for the 2001-2013 period.

Stations	Maximum AOD	Average LAI	Average NDVI
	1 st Peak (2 nd Peak)	1 st Peak (2 nd Peak)	1 st Peak (2 nd Peak)
Bac Giang	0.89/0.74	0.44/1.1	0.37/0.58
Chiang Mai	0.5/0.4	2.3/2.97	0.56/0.7
Mukdahan	0.53/0.44	0.96/1.62	0.45/0.67
Nghia Do	0.9/0.71	0.87/1.45	0.39/0.54
Pimai	0.5/0.46	0.54/1.22	0.42/0.61
Ubon Ratchani	0.51/0.46	1.09/1.14	0.48/0.55
Vientiane	0.62/0.59	2.13/2.39	0.52/0.63
Jambi	0.98	2.92	0.68
Kuching	0.66	4.16	0.75
Palangkaraya	1.05	3.72	0.68
Singapore	0.87	1.71	0.4

Figure 1. Domain with the two EOF regions highlighted and the location of the AERONET stations.

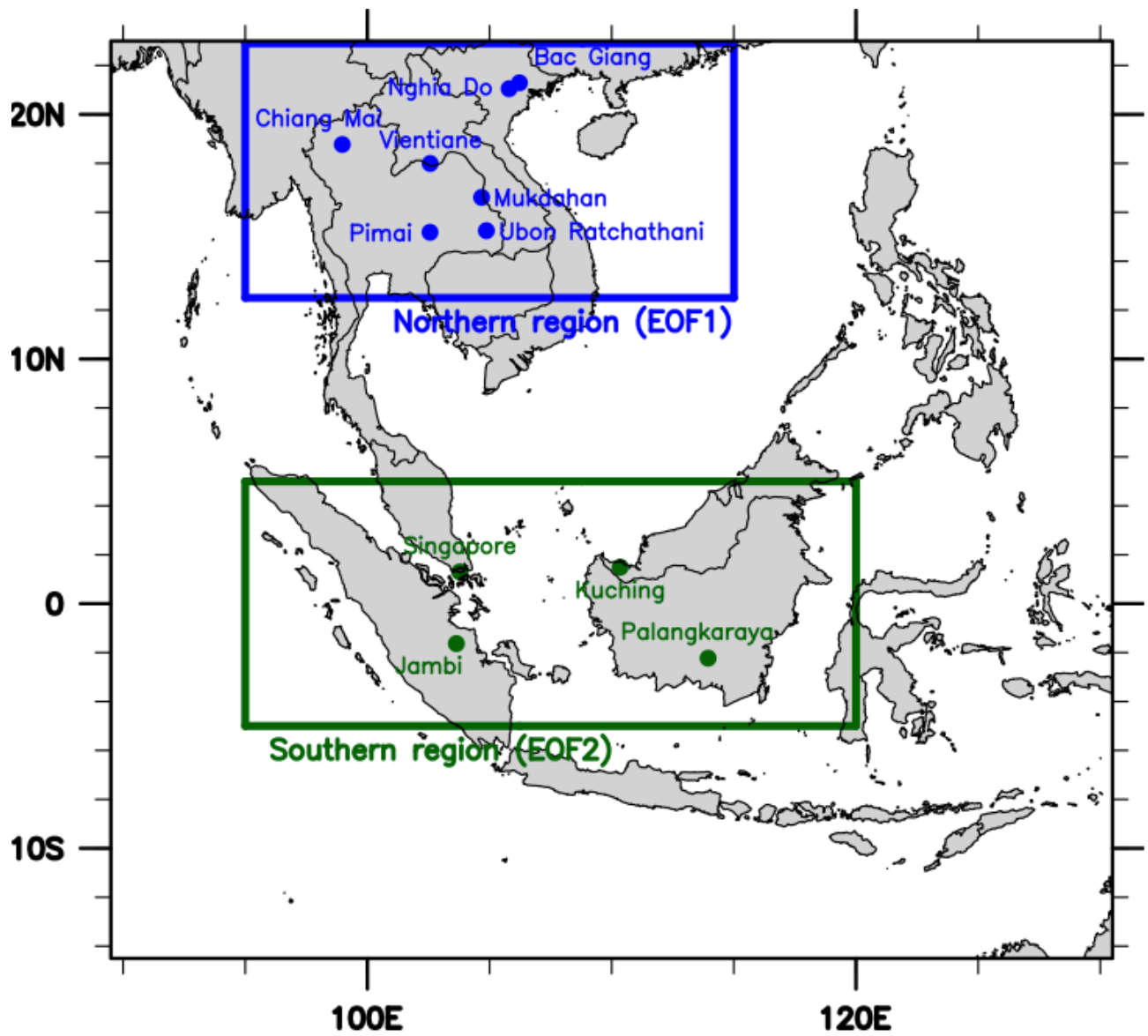


Figure 2. First line: EOF1 (38.2% of variance) (a) and EOF2 (13.3% of variance) (b) of the AOD (2001-2013). Regions of highest AOD variability are delineated by black dots. Second line: PC1 (cutoff 0.006, PC on the left hand axis, AOD on the right hand axis) (c) (red curve) and their associated AOD (green curve) averaged on the region. Third line: PC2 , (cutoff 0.01, PC on the left hand axis, AOD on the right hand axis) (d) (red curve) and their associated AOD (green curve) averaged on the region.

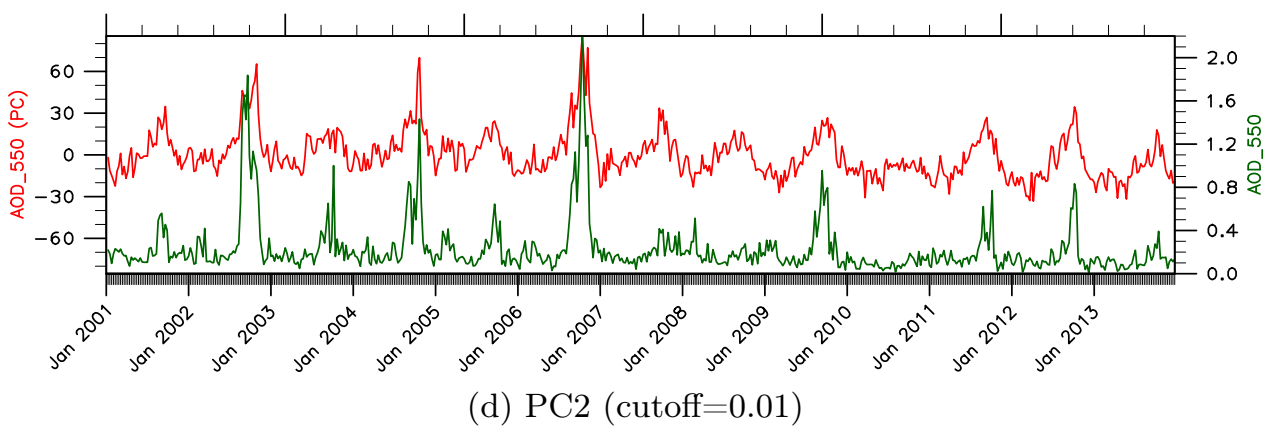
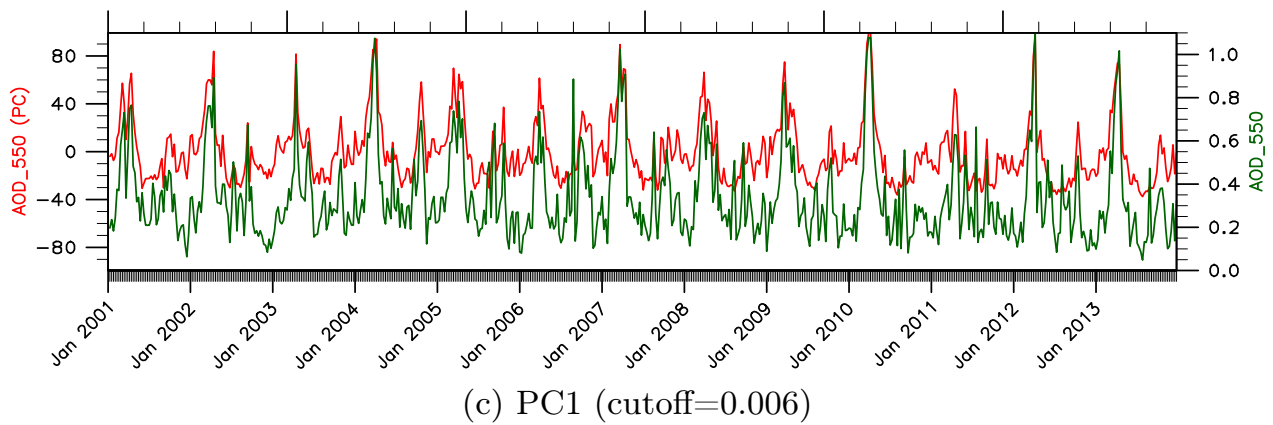
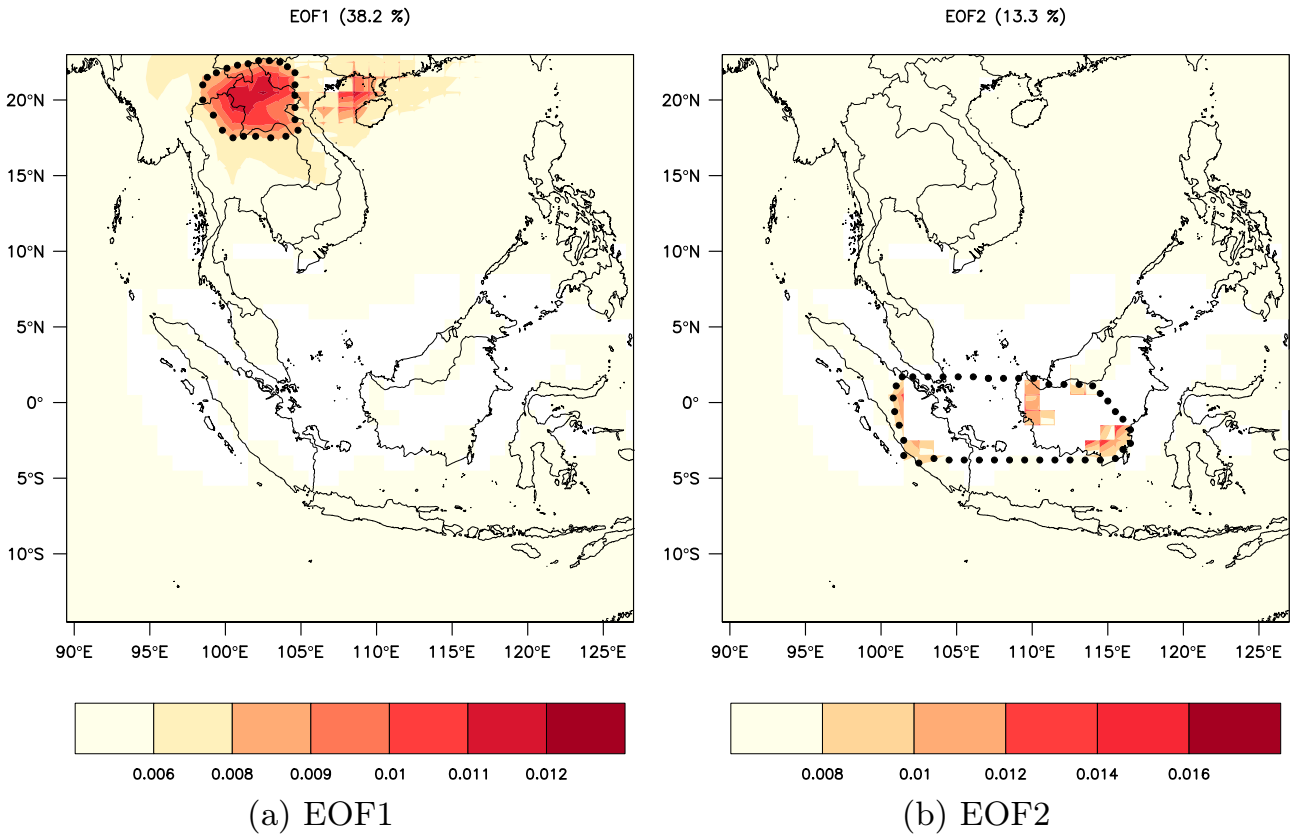


Figure 3. Climatological values of LAI (first column) and NDVI (second column) for the 2001–2013 period. Average values are displayed on the first line, while the standard deviation is displayed on the second line.

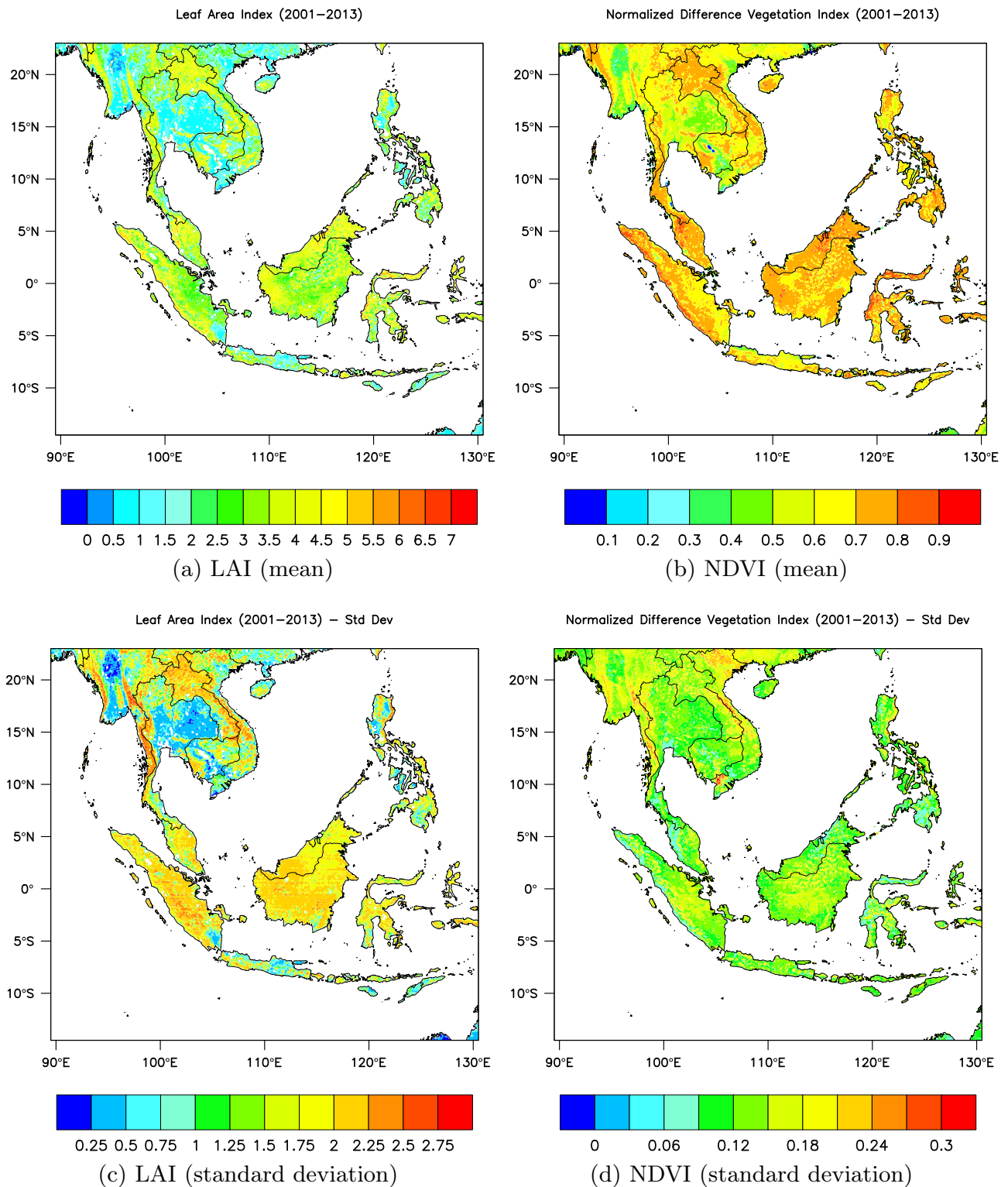


Figure 4. Regression Coefficients($\delta 1$) associated to Fire Count for REG1. Regions of highest AOD variability from the EOF analysis are delineated by black dots.

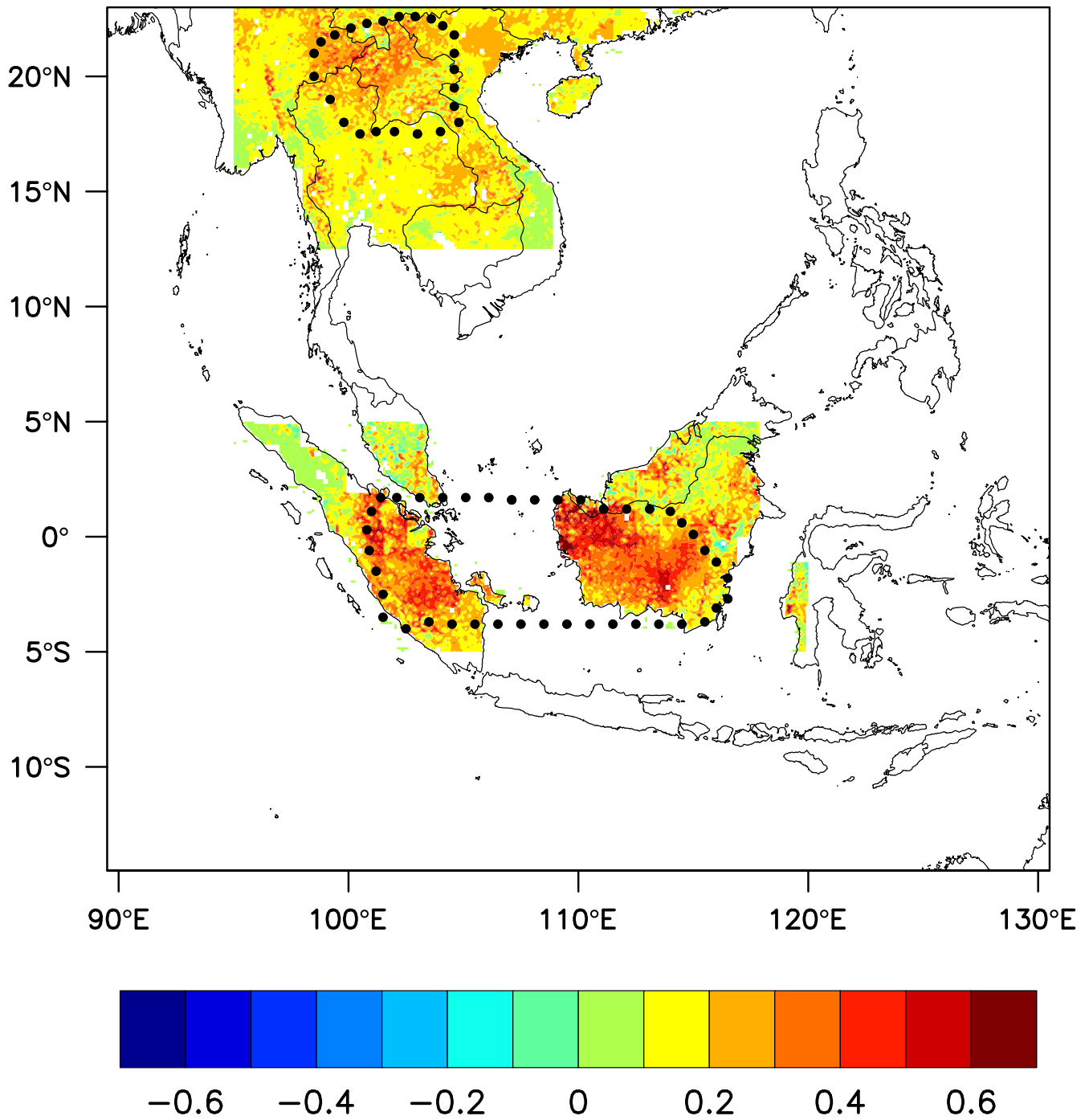
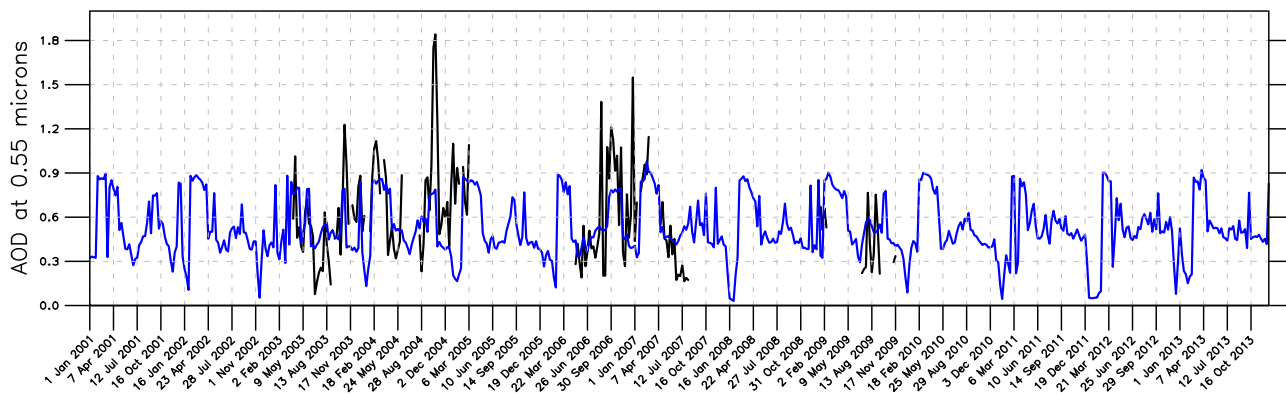
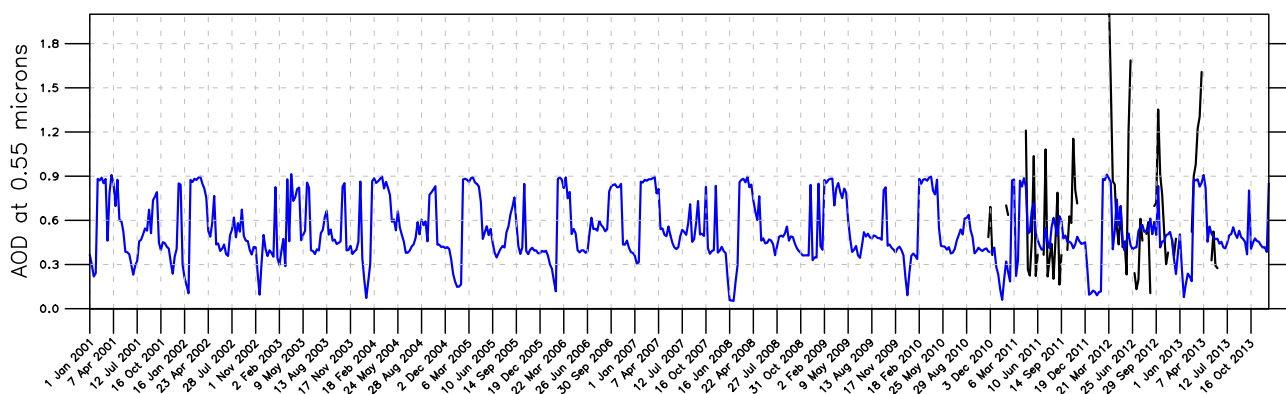


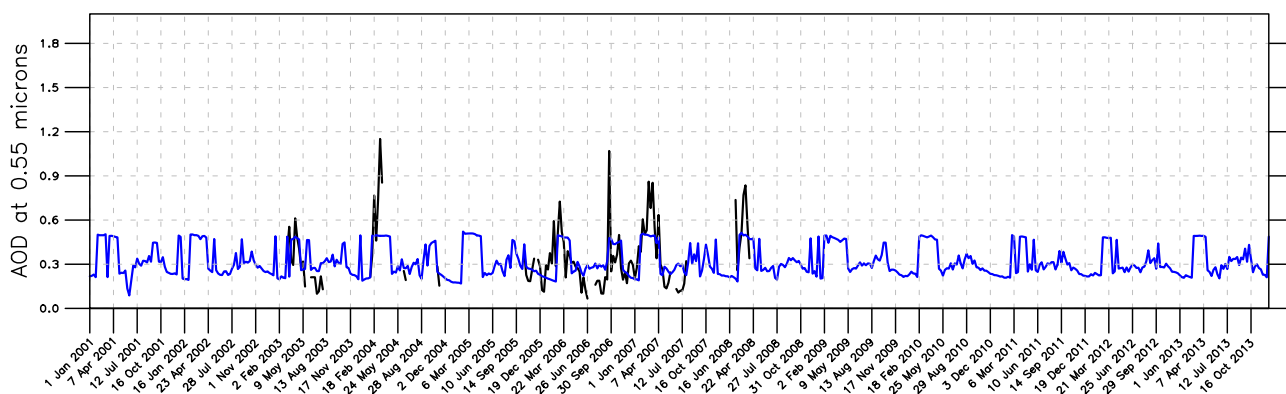
Figure 5. Temporal series of 8-day AERONET AOD (black) and AODNorth (blue) at Bac Giang (a1), Nghia Do (b1), Pimai (c1), Ubon Ratchathani (d1), Chiang Mai (a2), Mukdahan (b2), and Vientiane (c2) (2001-2013). All x-axes are the time coordinate from Jan 2001 through Dec 2013. All y-axes are the AOD.



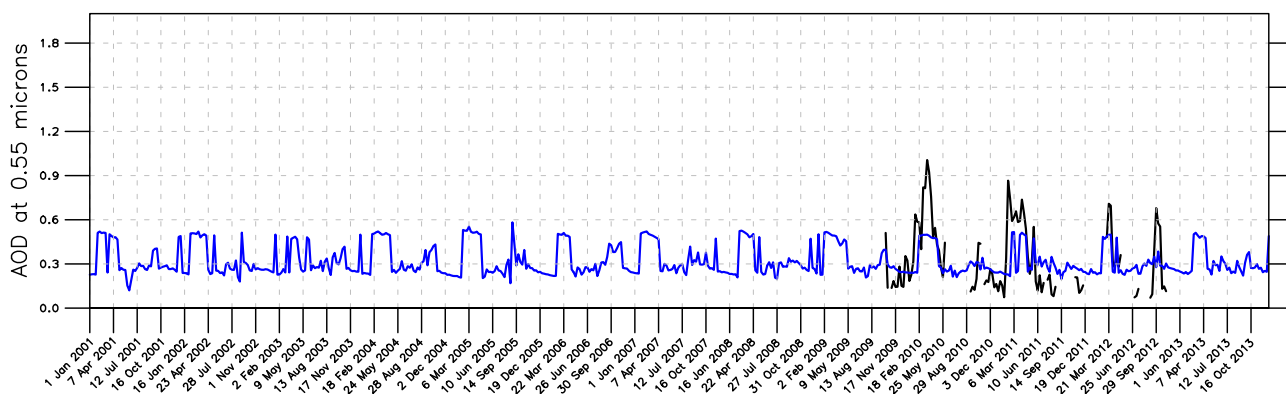
(a) Bac Giang



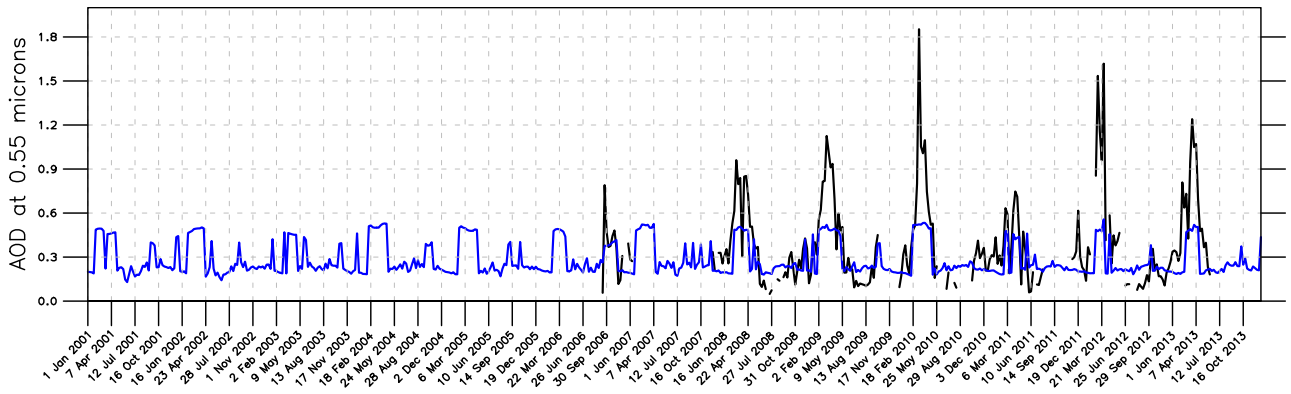
(b) Nghia Do



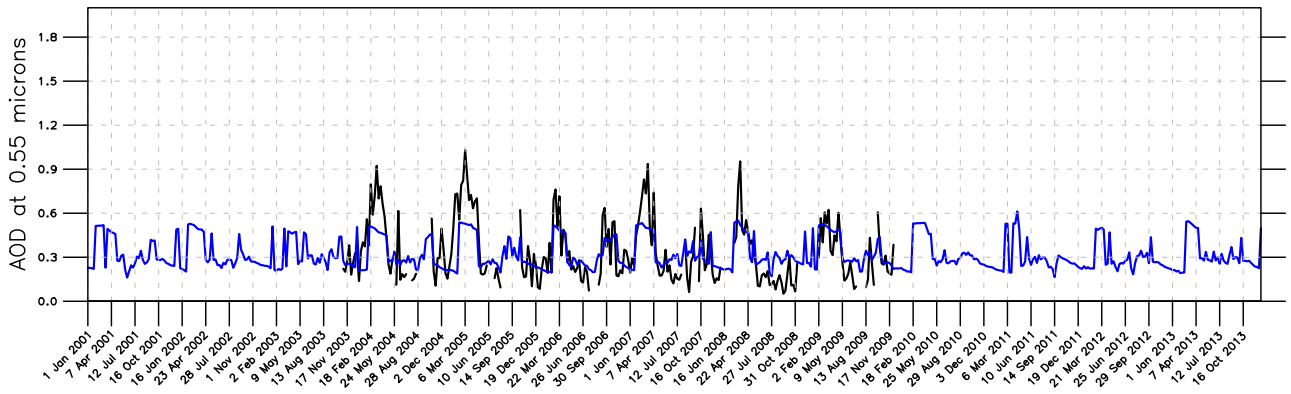
(c) Pimai



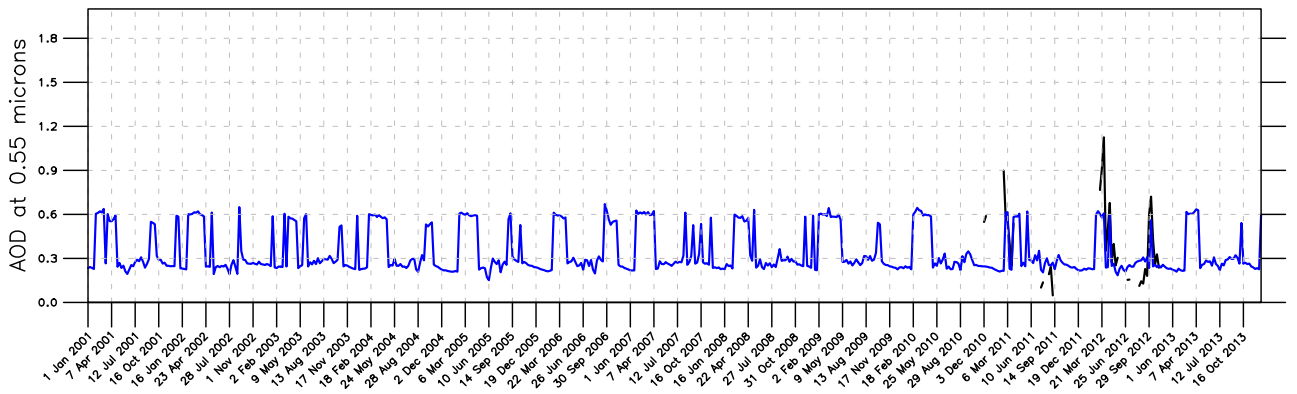
(d) Ubon Ratchathani



(a) Chiang Mai

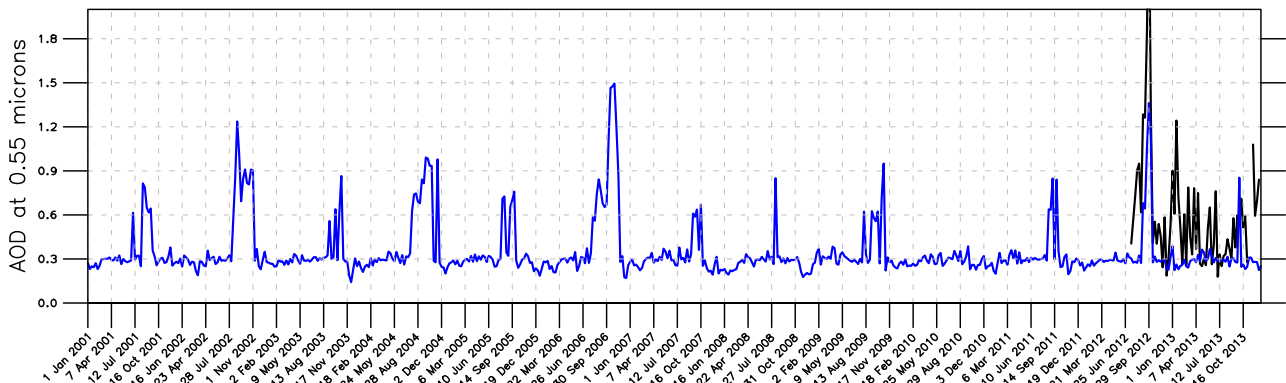


(b) Mukdahan

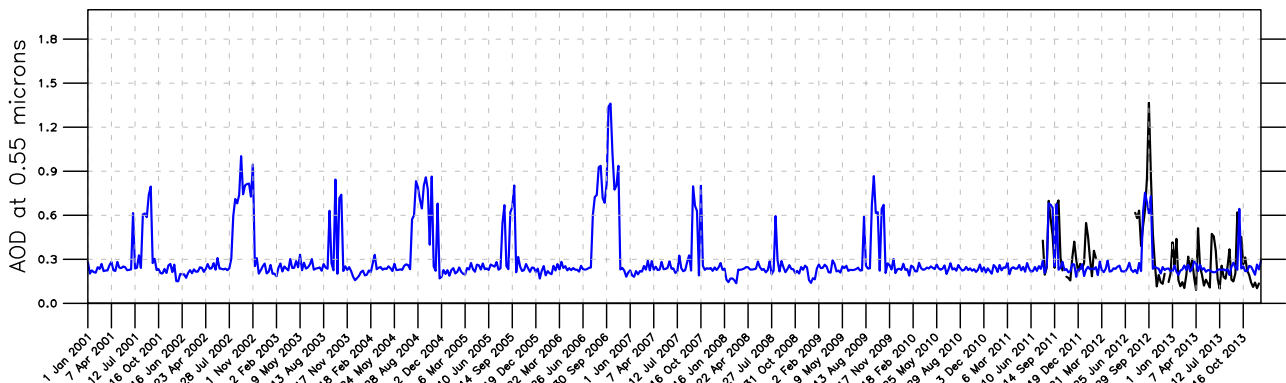


(c) Vientiane

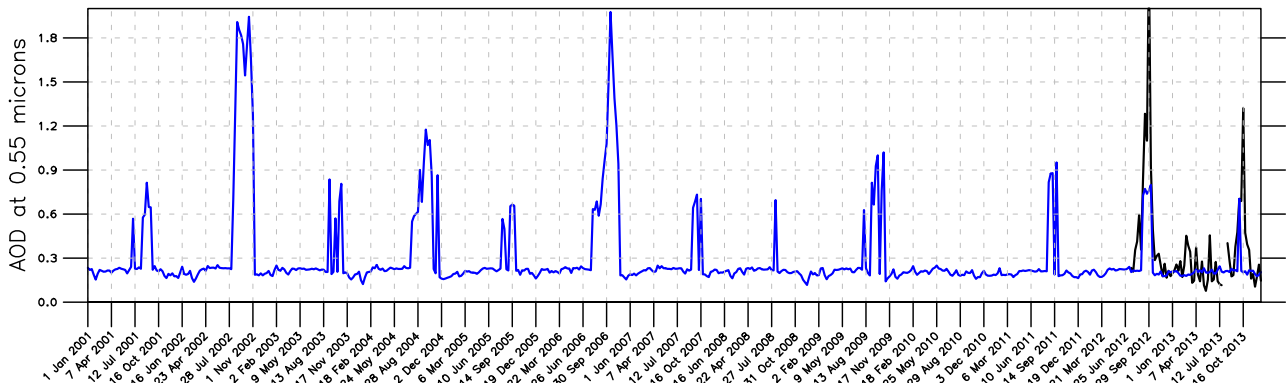
Figure 6. Temporal series of 8-day AERONET AOD (black) and AODSouth (blue) at Jambi (a), Kuching (b), Palangkaraya (c), and Singapore (d) (2001-2013).



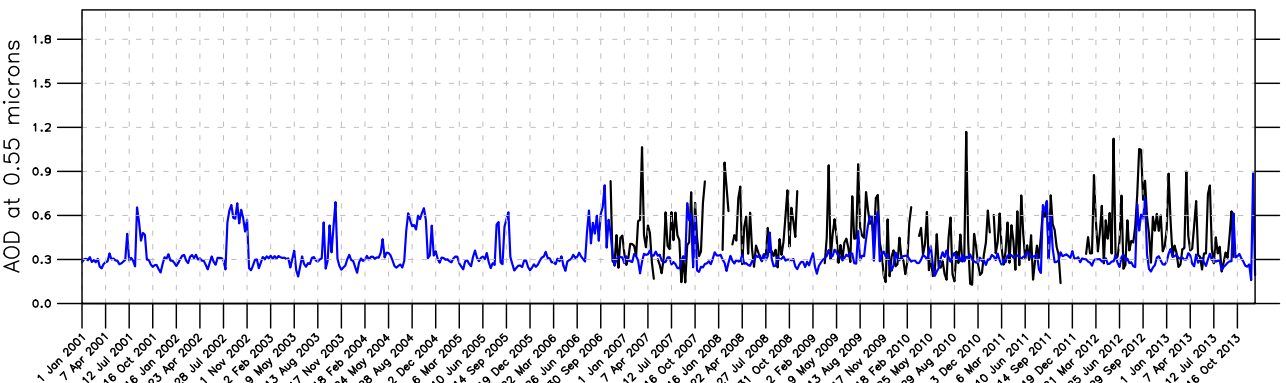
(a) Jambi



(b) Kuching



(c) Palangkaraya



(d) Singapore

Figure 7. Basic statistics between MISR and AODNorth (a,b) and AODSouth (a,b) on a monthly basis (2001-2013). Regions of highest AOD variability from the EOF analysis are delineated by black dots. Within the Northern Region the mean correlation is 84.8% and the average is 77.3% (mean error is 0.06), while in the Southern Region the mean correlation is 79.2% and the average is 72.4%(mean error is 0.08). The mean errors are given on the left hand side, while the correlations are given on the right hand side.

